Solar variability over the Holocene period

disentangling geomagnetic and solar influences on a new continuous 10Be record from Little Dome C, Antarctica

Nguyen, Hoang Long

2023

LUNDQUA THESIS 95

Solar variability over the Holocene period
– disentangling geomagnetic and solar influences on a new continuous ^{10}Be record from Little Dome C, Antarctica

LONG NGUYEN
QUATERNARY SCIENCES | DEPARTMENT OF GEOLOGY | LUND UNIVERSITY 2023

Printed by Media-Tryck, Lund 2023 NORDIC SWAN ECOLABEL 3041 0903


Sunset in Hanoi, the hometown of the author.

Quaternary Sciences
Department of Geology
Lund University
Sölvegatan 12
SE-223 62 Lund, Sweden
Telephone +46 46 222 78 80

ISSN 0281-3033
ISBN 978-91-87847-74-5

Lund University

LUNDQUA THESIS 95

Solar variability over the Holocene period

– disentangling geomagnetic and solar influences on a new continuous ^{10}Be record from Little Dome C, Antarctica

Long Nguyen

LUND UNIVERSITY

Quaternary Sciences

Department of Geology

DOCTORAL DISSERTATION

by due permission of the Faculty of Science, Lund University, Sweden.
To be defended at the Dept. of Geology, Lund University, on the 21st of April 2023 at 13:15.

Faculty opponent
Thomas Laepple

Alfred Wegener Institute, Germany

Front cover: Long Nguyen

Back cover: qdnd.vn

Quaternary Sciences
Department of Geology
Faculty of Science

ISBN 978-91-87847-74-5 (print)
ISBN 978-91-87847-75-2 (pdf)
ISSN 0281-3033

Printed in Sweden by Media-Tryck, Lund University, Lund 2023

Media-Tryck is a Nordic Swan Ecolabel certified provider of printed material. Read more about our environmental work at www.mediatryck.lu.se

MADE IN SWEDEN

<table>
<tr><td colspan="2">Organization

LUND UNIVERSITY
Department of Geology
Sölvegatan 12
SE-223 62 Lund
Sweden

Author: Long Nguyen</td><td colspan="2">Document name

DOCTORAL DISSERTATION

Date of issue: 21st April 2023

Sponsoring organization</td></tr>
<tr><td colspan="4">Title and subtitle: Solar variability over the Holocene period – disentangling geomagnetic and solar influences on a new continuous ^{10}Be record from Little Dome C, Antarctica</td></tr>
</table>

Abstract:

Reliable information on solar activity over the Holocene period is important to predict the Sun in the future and to understand the mechanism behind the Sun-climate linkage. Presently, there are discrepancies in the proxy data of solar activity due to reasons that are not yet understood. This leads to major uncertainties in Holocene solar reconstructions. This PhD project aims to improve the Holocene solar reconstructions with a new dataset and a better reconstruction method. The results are be important for solar and Sun-climate studies as well as for a better understanding of past changes in the carbon cycle.

Cosmogenic radionuclides such as ^{10}Be in ice cores and ^{14}C in tree rings are the best-known proxies for solar activity far back in time. The radionuclide records reflect a combination of production, transportation and deposition processes (atmospheric circulation (^{10}Be) and carbon cycle (^{14}C)). Presently, the different radionuclide records show disagreements regarding their long-term (millennial-scales) changes for unknown reasons. Moreover, the radionuclide records are also influenced by long-term changes in the geomagnetic field that are not well constrained. This leads to major uncertainties in reconstructions of past changes in solar activity.

This thesis is based on new ^{10}Be measurements from 759 ice chip samples drilled at the East Antarctic site called Little Dome C (LDC). The new ^{10}Be record continuously covers the entire Holocene. A Bayesian model was also developed to disentangle solar activity and geomagnetic field influences on the radionuclide records. The model was applied on the new LDC ^{10}Be data and also on the existing ^{10}Be data from other ice cores and tree-ring ^{14}C data. The reconstructions show consistent short-term variations (decadal- and centennial-scale) of solar activity while long-term variations (multi-millennial-scale) are still uncertain. Long-term discrepancies are present among the ^{10}Be records and the ^{14}C data, especially for the last 4 ka. We also found hints of a polar bias effect that dampens the geomagnetic field influence on Antarctic ^{10}Be records but the effect is absent in a Greenland ^{10}Be record. These results point to a difference in the transportation mode of ^{10}Be toward the different ice core sites and an influence of the carbon cycle changes on the ^{14}C data.

Key words: Ice core, cosmogenic radionuclide, 10Be, 14C, solar activity, paleomagnetism, Holocene		
Classification system and/or index terms (if any)		
Supplementary bibliographical information		**Language:** English
ISSN and key title: 0281-3033 LUNDQUA THESIS		**ISBN:** 978-91-87847-74-5
Recipient's notes	**Number of pages:** 118	Price
	Security classification	

Signature Date 2023-03-06

Contents

List of papers

Paper I

Nguyen, L., Paleari, C., Müller, S., Christl, M., Mekhaldi, F., Gautschi, P., Mulvaney, R., Rix, J., Muscheler, R., 2021. The potential for a continuous 10Be record measured on ice chips from a borehole. Results in Geochemistry 5, 100012, doi: 10.1016/j.ringeo.2021.100012. *Available in open access*.

Paper II

Nguyen, L., Suttie, N., Nilsson, A., Muscheler, R., 2022. A novel Bayesian approach for disentangling solar and geomagnetic field influences on the radionuclide production rates. Earth, Planets and Space 74, 130, doi: 10.1186/s40623-022-01688-1. *Available in open access*.

Paper III

Nguyen, L., Suttie, N., Nilsson, A., Müller, S., Christl, M., Gautschi, P., Mulvaney, R., Rix, J., Muscheler, R.,. No evidence for multi-millennial scale variations of solar activity during the Holocene constrained from cosmogenic radionuclides. *Manuscript*.

Acknowledgement

The Sun is such a fascinating topic not only in science but also in the literature. I bet we all at some point in our lives have heard the song "*You are my sunshine*". I have such an amazing PhD project where I can study the Sun. And of course it cannot happen without my supervisor Raimund. Thank you for such a wonderful opportunity and for your support/supervision during the four years of my study. I cannot stress enough how much it means to me especially during the COVID-19 pandemic. I also deeply appreciate the help and support of my co-supervisors Andreas and Florian. Thank Andreas for your help with the Swedish summary.

Many thanks to my friends who have made my life in Sweden so much more interesting. A big thank you to my fellow PhD students who have made the office way more fun. I would like to thank Florian and Chiara for helping and keeping me company when I was new in Sweden and knew no one. And to the badminton team Minjie, Jesper, Hans and Mats, thank you for teaching me how to play badminton with so much patience.

I also want to acknowledge the Royal Physiographic Society of Lund for their generous funding for my sample measurements and conference travelling.

Finally, I am truly grateful for the support of my wife, my cat and my family. I would like to thank my cat Max (picture below) for keeping me company while I am editing these lines at nights. Thank you, my beautiful wife Trang, who is always there for me, sharing, caring and helping me through tough times. *Em là ánh nắng của anh!*

Cảm ơn và Trân trọng / Thanks & Best Regards!

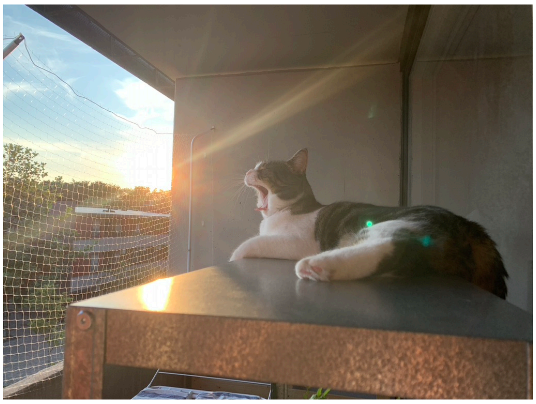

Praise the Sun!

Abbreviations

AMS	Accelerator mass spectrometry
BP	Before Present (1950)
CMEs	Coronal Mass Ejections
EDC	Epica Dome C
EDML	EPICA Dronning Maud Land
GCRs	Galactic cosmic rays
GDM	Geomagnetic Dipole Moment
GPS	Global Positioning System navigation
GRIP	Greenland Ice Core Project
GISP2	Greenland Ice Sheet Project 2
GSN	Group Sunspot Number
IECs	Ion Exchange columns
LDC	Little Dome C
MCMC	Markov Chain Monte Carlo
VADM	Virtual axial dipole moment
WAIS	Western Antarctic Ice Sheet

1 Introduction

Life and the climate system on the Earth are fuelled by the Sun. It is an active star with variations on different timescales that have been revealed by spacecraft measurements and by observing the number of sunspots (i.e. dark spots occurring on the Sun's surface). The solar magnetic field varies with time driving different aspects of solar activity. The information on past solar activity is of special interest for prediction of the range and variations of future solar activity and to study the Sun-climate linkages (e.g. Gray et al., 2010). Unfortunately, reliable information provided by direct observations goes only back to the 1600s (i.e. when the telescope-based sunspot observations started). Information on solar variability longer than 400 years has to rely on indirect proxy data obtained from geological archives.

Cosmogenic radionuclides such as ^{10}Be in ice cores and ^{14}C in tree rings are the best-known proxies for solar activity prior to 1600s (Lal & Peters, 1967; Muscheler et al., 2007). They are produced by the interaction of galactic cosmic rays (GCRs) with atoms in the atmosphere and are transported/deposited afterwards via various pathways to their natural archives, e.g. ice cores and tree rings (Field et al., 2006; Laj et al., 2002; Muscheler et al., 2004). The GCRs, prior to reaching the atmosphere, can be deflected by the shielding effects of the solar and the Earth's magnetic fields (Masarik & Beer, 1999, 2009). Thus, the number of cosmogenic radionuclides found in their natural archives varies as a consequence of solar activity and geomagnetic field variability and climate impacts on the transport/deposition processes.

Reconstructions of past solar activity from the radionuclide records, therefore, require the correction for the effects of transport/deposition processes and geomagnetic field variability. Since these processes are not always well understood, uncertainties associated with the correction are inevitable. Presently, there are discrepancies between ^{10}Be records from Greenland and Antarctic ice cores, and also between ^{10}Be and ^{14}C records regarding their millennial-scale changes over the Holocene (the last ~11.7 ka) for unknown reasons (Muscheler et al., 2016; Steinhilber et al., 2012; Vonmoos et al., 2006; Wu et al., 2018). This leads to major uncertainties in the reconstruction of Holocene solar activity. On the other hand, the reconstructions of millennial-scale solar activity require long-term ^{10}Be records which are available from the Greenland Ice Core Project (GRIP, Vonmoos et al., 2006), the Greenland Ice Sheet Project 2 (GISP2, Finkel & Nishiizumi, 1997), the EPICA Dronning Maud Land project (EDML, Steinhilber et al., 2012) at East Antarctica and the Western Antarctic Ice Sheet ice core (WAIS, Sigl et al., 2016). Unfortunately, these records are not covering the entire Holocene epoch including the instrumental era (i.e. after the 1900s when ^{10}Be production rate is well constrained from measurements). Therefore, the connection of ^{10}Be from these deep ice cores to the atmospheric production rate carries additional uncertainties. Another major source of uncertainty is the influence of geomagnetic field variability on the radionuclide production which is not well constrained at the moment (Korte & Muscheler, 2012; Snowball & Muscheler, 2007; Vonmoos et al., 2006).

The main objective of this PhD project is to improve solar activity reconstructions over the Holocene with focus on long-term changes (centennial- to millennial-scale). To achieve this (i) we measured a new ^{10}Be record covering the entire Holocene epoch from a site called Little Dome C (LDC, 75.36°S and 122.42°E), at a distance of approximately 40 km from the Dome Concordia station in East Antarctica. The data here is expected to be less disturbed by local climate influences than the existing ^{10}Be records due to a low snow accumulation (~2 cm/year) at the site (Rowell et al., 2022). This might help to understand the present discrepancies between Greenland and Antarctic ^{10}Be records which are likely due to the differences in the transport and deposition of ^{10}Be to the ice caps (Pedro et al., 2011). Moreover, the new LDC record covers the entire Holocene period until to today and therefore helps improve the coverage of the global ^{10}Be data set and facilitates the connection to the present ^{10}Be production rate. Thus, the new LDC record is important for an improved and complete reconstruction of Holocene solar activity. (ii) This thesis also aims to improve the method of solar reconstruction via developing and applying a novel statistical method to disentangle and reconstruct solar activity and geomagnetic field variability from the radionuclide data. The current reconstruction methods are purely numerical and neglect the information on the known characteristic variations of solar activity and the geomagnetic field. Here, I present a novel Bayesian model that utilises and accounts for such information and through that minimises the impacts of noise in the radionuclide data and the uncertainty associated with the geomagnetic field shielding. Moreover, the model's ability to reconstruct geomagnetic field variability from the radionuclide data creates an opportunity to evaluate the model reconstruction via comparisons with independent geomagnetic field reconstructions based on paleomagnetic data.

2 Background

2.1 Solar activity

The Sun is a variable star. Direct observations (such as by spacecraft) have shown that the properties of the solar magnetic field vary with time and drive other aspects of solar variability such as solar flares (i.e. intense bursts of radiation, figure 2.1a), coronal mass ejections (CMEs, i.e. eruption of large plasma clouds carrying magnetic fields, figure 2.1b) and high-speed solar winds (Beer et al., 2012; NASA, 2017). This can cause extreme variability in the so-called space weather with potentially significant impacts on our modern society. For example, geomagnetic storms can disrupt electric power grids, solar flares can interfere with high-frequency radio communication and Global Positioning System navigation (GPS), and energetic particle events can harm spacecraft electronics as well as human and robotic explorers across the solar system (NASA, 2017). In addition, there is evidence of long-term solar activity driving changes in the Earth's climate system, even though the exact forcing mechanisms involved are unclear (e.g. Gray et al., 2010 and references therein).

The level of solar activity can be estimated directly by telescopic observations and counting the number of sunspots (Clette & Lefèvre, 2016; Wolf, 1851, 1856) or the number of groups of sunspots denoted as group sunspot number (GSN, Hoyt & Schatten, 1998; Svalgaard & Schatten, 2016). Sunspots are relatively dark spots representing regions with strong, ephemeral magnetic fields on the Sun's photosphere (NASA, 2017). They can also appear together as a group (figure 2.2). Solar activity is considered to be strong if more sunspots are present on the Sun's surface and vice versa. With increasing sunspot number, solar events such as CMEs occur more frequently which will generate strong and turbulent solar winds (Beer et al., 2012; Owens & Forsyth, 2013). On the contrary, there are fewer CMEs at minimal sunspot numbers and the solar wind is relatively calm.

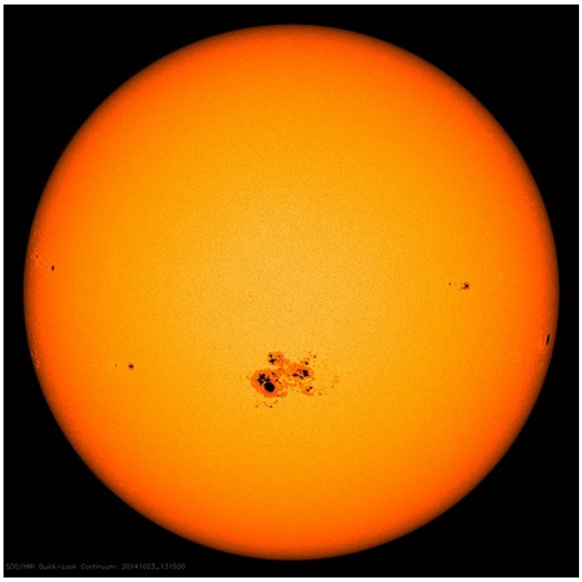

Figure 2.2: A picture of a sunspot group (the cluster of dark spots) in 2014. *Credit: NASA/SDO*

Sunspot numbers are the longest records of direct solar observations which are continuous since 1610 CE. These continuous records (e.g. GSN in figure 2.3) have indicated important features of solar activity such as the 11-year Schwabe cycle (Schwabe, 1844). In addition, there are extended periods of very low sunspot number which are referred to as Grand Minima. Example of those Grand Minima (i.e. Maunder and Dalton Minima) are shown in the figure 2.3.

Another way to estimate solar activity is through the modulation effects on the galactic cosmic rays (GCRs) in the heliosphere. Upon entering the solar system, the GCRs drift within and are deflected by the

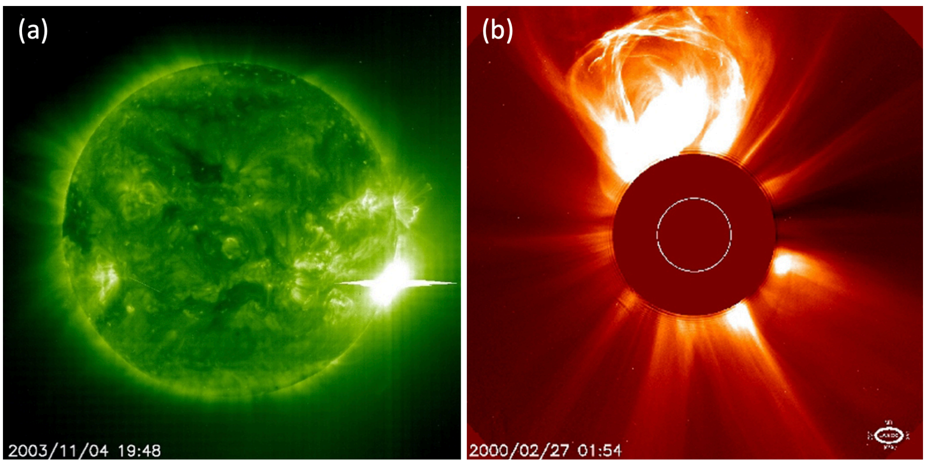

Figure 2.1: Expressions of solar activity, i.e. (a) a powerful solar flare in 2003 and (b) a CME in 2000 captured by SOHO spacecraft. *Credit: ESA & NASA/SOHO*

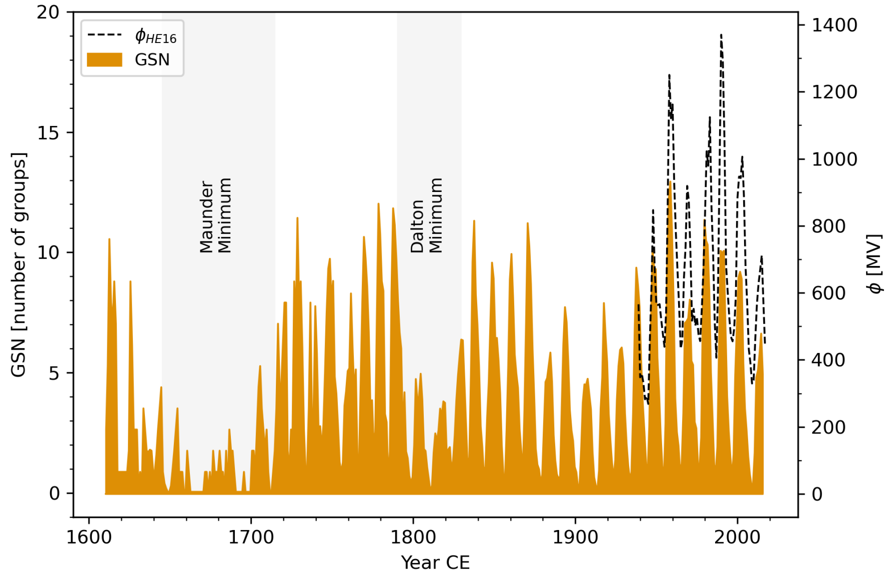

Figure 2.3: (Left axis) Yearly mean of GSN (1610 – 2016 CE; Svalgaard & Schatten, 2016) and (right axis) a recent record of solar modulation potential ϕ_{HE16} (1939 – 2017 CE; Herbst et al., 2017) inferred from neutron monitor. Known solar minima during the period are also indicated by the grey bars.

solar magnetic field that is carried by the solar winds (Beer et al., 2012). Strong solar activity associated with turbulent solar winds leads to enhanced deflection which will result in less GCRs reaching the Earth. This process is often referred to as solar modulation. The modulation processes including convection, drifts, diffusion and adiabatic energy changes are described by the GCR transport equation (Parker, 1965). A simplified approach is the force-field approximation (Caballero-Lopez & Moraal, 2004; Gleeson & Axford, 1968; Moraal, 2013) which uses a single parameter to approximate the solar modulation:

$$\frac{j(r,E)}{E^2-E_0^2} = \frac{j_{lis}}{(E+\Phi)^2-E_0^2} \tag{2.1}$$

where j is the observed GCR intensity at radial distance r, j_{lis} is the local interstellar spectrum (LIS), E is total energy and Φ is the solar modulation function. Φ [MeV] describes the energy loss of the GCR due to the modulation processes and it is given by:

$$\Phi = Ze\phi \tag{2.2}$$

where ϕ [MV] is the modulation potential (or modulation parameter) and Ze is the electrical charge of the particle. ϕ is therefore a direct measure of solar activity and it can be determined via monitoring the GCR coming to the Earth. For example, the neutron monitor method measures the non-thermal neutron component of the nucleonic cascade initiated by GCR in the Earth's atmosphere (Simpson, 2000). Figure 2.3 shows a recent record of solar modulation potential ϕ_{HE16} (1939 – 2017 CE) inferred from the neutron monitor data using an updated LIS inferred from Voyager1 spacecraft data (Herbst et al., 2017). ϕ_{HE16} exhibits a strong 11-year cycle and is significantly correlated to the GSN record indicating a strong solar modulation when the Sun is active.

2.2 The geomagnetic field shielding

The GCR flux coming to the Earth is also modulated by the geomagnetic shielding depending on the angle of the incidence, the latitude where the GCR are heading to, and the intensity of the geomagnetic field (Masarik & Beer, 1999, 2009). At a distance of several Earth radii (where the modulation occurs) the geomagnetic field is predominantly dipolar and axisymmetric. In general, the shielding effect is strongest at the equator and when the GCRs are coming from the eastern horizon. On the other hand, there is low to no shielding effect around polar regions because the geomagnetic field lines are almost perpendicular to the Earth's surface. In addition, the geomagnetic field intensity can vary on centennial- and millennial-timescales (Constable & Korte, 2015; Korte & Muscheler, 2012; Panovska et al., 2019) which also influences the GCR flux arriving at the Earth's atmosphere.

The geomagnetic field also contains non-dipolar field components, which are important for describing the geomagnetic field at the Earth's surface, although the axisymmetric dipole field component is thought to have been dominant for most of the geological history (Panovska et al., 2019). Information of past variations of the geomagnetic field, i.e. paleomagnetic data (declination, inclination and intensity measurements), can be obtained from lake and marine sediments, volcanic rocks and archaeological materials. The geomagnetic data are used to construct global varying geomagnetic field models (e.g. Constable et al., 2016; Nilsson et al., 2022; Pavón-Carrasco et al., 2014) that separate the different dipole and non-dipole field contributions to, for example, calculate the strength of the dipole component, i.e. geomagnetic dipole moment (GDM). Alternatively, a virtual axial dipole moment (VADM) can be reconstructed via averaging global absolute paleointensity data assuming that the geomagnetic field consisted of only an axisymmetric dipole field, i.e. aligned with the Earth's rotation axis (Knudsen et al., 2008; Yang et al., 2000). Presently, there are significant disagreements between the reconstructions (e.g. figure 2.4) leading to poor constraint of the GDM during the Holocene epoch.

A persistent north-south hemispheric asymmetry is present in GDM reconstructions for the past few thousand years with generally lower field intensity in the southern hemisphere (Constable & Korte, 2015; Nilsson et al., 2022). The lower field intensity could lead to differences in the geomagnetic shielding between the hemispheres during the Holocene. However, reconstructing north-south asymmetries in the field is challenging due to the sparse data distribution especially in the southern hemisphere (e.g. Gallet et al., 2009) and more work needs to be done to constraint such features of the geomagnetic.

2.3 Reconstruction of long-term solar activity from cosmogenic radionuclides

2.3.1 Cosmogenic radionuclides an indirect proxy of solar activity

The Sun is more than 4.5 billion years old (Bonanno et al., 2002). Solar activity at timescales longer than 400 years cannot be captured by the GSN. Long-term reconstructions need to rely on indirect proxy data obtained from geological archives such as ^{10}Be from ice core and ^{14}C from tree rings. These natural archives can survive and preserve the radionuclides for thousands up to hundreds of thousands of years.

High-energy GCRs that have passed through the solar system and the geomagnetic shield will trigger a cascade of reactions upon entering the Earth's atmosphere. In some instances, cosmogenic radionuclides (e.g. ^{10}Be and ^{14}C) are produced by those reactions (Beer et al., 2012). The production rate of cosmogenic radionuclides depends on the amount of GCR entering the Earth's atmosphere which in turn is influenced by three main factors, i.e. the GCR flux outside the heliosphere, solar activity and the shielding effect of the Earth's magnetic field. Although the geomagnetic field contains non-dipole components at fine scale, the global production rate is mostly sensitive to the changes in the GDM. The effects of the nondipole components on the production rate are usually averaged out over large spatial and long timescales (Panovska et al., 2019). The production rate can therefore be linked directly to ϕ and GDM. The GCR flux coming to the solar system

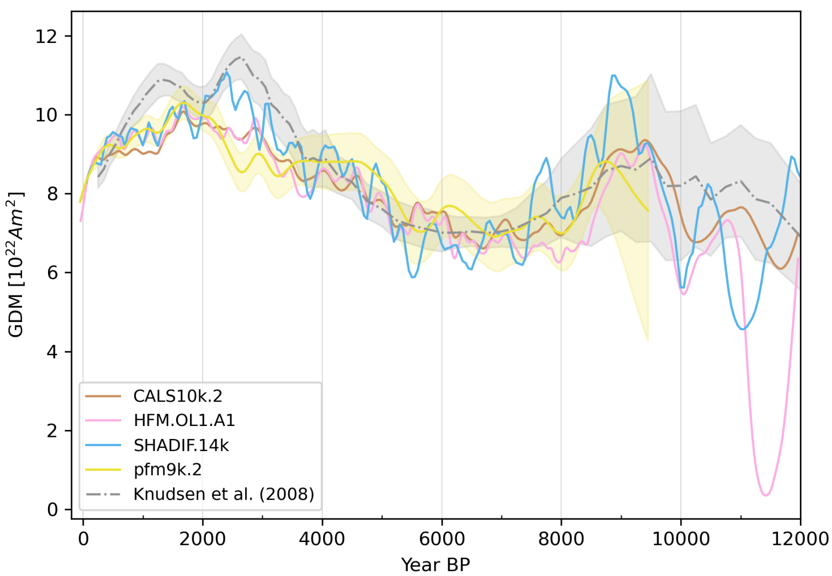

Figure 2.4: A comparison of GDMs reconstructed by various geomagnetic models, i.e. CALS10k.2 and HFM.OL1.A1 (Constable et al., 2016), SHADIF.14k (Pavón-Carrasco et al., 2014), pfm9k.2 (Nilsson et al., 2022) and a VADM reconstructed by Knudsen et al. (2008). The shadings (in corresponding colours) indicate 2-σ uncertainty of the pfm9k.2 and the VADM.

is constant within ±10% during the last ~10 million years as indicated by meteorite investigations and terrestrial evidence (Wieler et al., 2013). Meanwhile, solar activity can vary significantly on decadal- to centennial-scale (Bond et al., 2001; Damon & Sonett, 1991; Gleissberg, 1965; Gleissberg & Schove, 1958; Knudsen et al., 2009; Schwabe, 1844; Sonett & Suess, 1984; Steinhilber et al., 2012; Wagner et al., 2001) and the GDM can vary on centennial- and millennial-scales (Constable & Korte, 2015; Korte & Muscheler, 2012; Panovska et al., 2019). Together, solar and geomagnetic variability induces major short- and long-term changes in the radionuclide production rates. Figure 2.5 shows the effects that solar modulation (quantified by ϕ) and the GDM (M) have on the global average of (a) ^{10}Be production rate (Kovaltsov & Usoskin, 2010) and (b) ^{14}C production rate (Kovaltsov et al., 2012). The calculation was conducted using models that simulate cosmic ray particle interactions with the Earth's atmosphere. The production rate is highest in the absence of solar shielding and low M. The production rate decreases non-linearly with increasing ϕ and M.

After being produced, ^{10}Be attaches to aerosols and is removed from the atmosphere by dry/wet deposition to end up in environmental archives like ice caps (Field et al., 2006). The removal process in the stratosphere (~1 year) is much slower than in the troposphere (~few weeks) owing to the stable stratification with much less vertical transport in the stratosphere (Heikkilä et al., 2009; Jordan et al., 2003; McHargue & Damon, 1991; Raisbeck et al., 1981a). Therefore, the stratospheric ^{10}Be is expected to be globally well-mixed while the tropospheric ^{10}Be is expected to carry a mostly regional signal. Consequently, ^{10}Be concentrations in ice cores can consist of a global stratospheric signal and a regional tropospheric production rate signal. Several studies have suggested an enhanced signal of the polar production rate compared to the global average production rate in ^{10}Be data from polar ice cores, a pattern known as the "polar bias" (Adolphi et al., 2023; Bard et al., 1997; Field et al., 2006; Heikkilä et al., 2009; McCracken, 2004; Pedro et al., 2012; Steig et al., 1996). This bias enhances the signal of solar activity and dampens the GDM influence due to the low geomagnetic shielding in the polar regions. However, there is no consensus regarding the presence and significance of the polar bias. The latest study (Adolphi et al., 2023) compared results from circulation models with independent ^{10}Be datasets and showed that the GDM signal for the Laschamps geomagnetic field minimum (~41 ka BP) was suppressed by 23% to 27% in polar ice core ^{10}Be. Meanwhile, the solar activity signal was enhanced by only 7% to 8%. However, the presence of the polar bias during the Holocene is still inconclusive due to a mismatch between the GDM variations and the differences in the ice core ^{10}Be. In addition, changes in the global atmospheric circulation or the regional precipitation could also affect the ^{10}Be concentrations (Field et al., 2006; Heikkilä et al., 2014; Heikkilä & Smith, 2013; Pedro et al., 2006, 2011, 2012). Overall, ^{10}Be records from polar ice cores reflect a mixed signal from the production, transport and deposition processes and so they are not exactly proportional to the global ^{10}Be production rate.

After being produced ^{14}C oxidizes to $^{14}CO_2$ and enters the carbon cycle (Laj et al., 2002; Muscheler et al., 2004). $^{14}CO_2$ from the atmosphere is assimilated by trees and is then stored as carbon in the trunk, branches, leaves and roots. Thus, analysing tree rings can give information about the atmospheric concentration of ^{14}C in the past which can be used to reconstruct past solar activity. The atmospheric concentration retrieved from tree rings largely represents the global atmospheric ^{14}C concentration due to the long atmospheric residence time (~5 years)

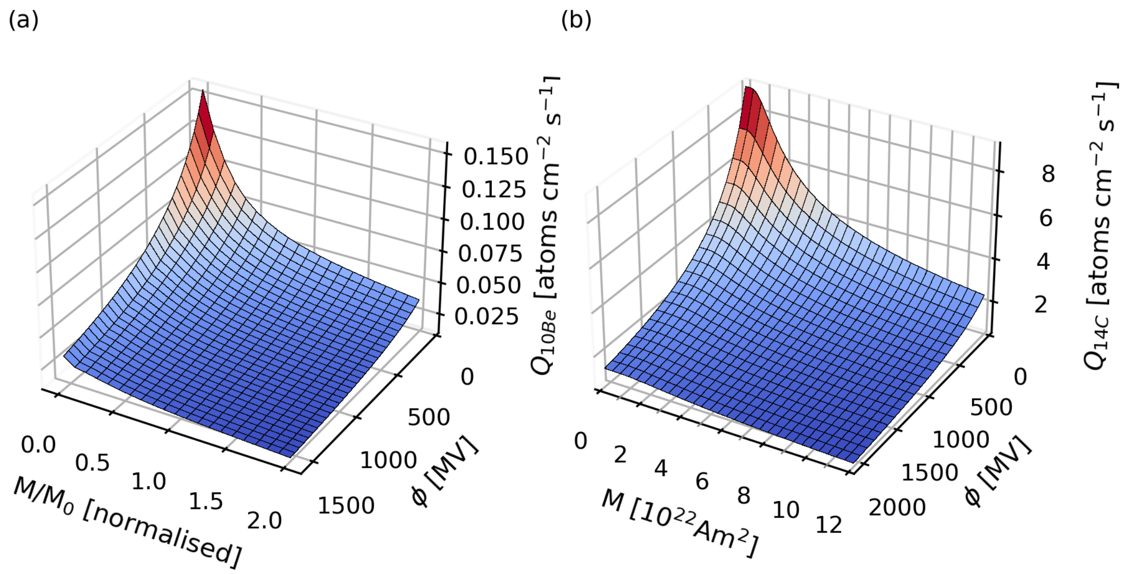

Figure 2.5: Global average production rate of (a) ^{10}Be and (b) ^{14}C as a function of the solar modulation potential (ϕ) and geomagnetic dipole moment (M) adapted from Kovaltsov & Usoskin (2010) and Kovaltsov et al. (2012), respectively. M in subpanel (a) was normalised to today's value M_0.

and efficient mixing of $^{14}CO_2$ (Muscheler et al., 2007). However, changes in the carbon cycle i.e. redistribution of CO_2 among the reservoirs (i.e. atmosphere, biosphere and oceans) could alter the atmospheric concentration of $^{14}CO_2$ and induce system effects into the ^{14}C data of tree rings (Laj et al., 2002; Muscheler et al., 2004, 2007).

2.3.2 Current state of Holocene solar reconstructions from ice core ^{10}Be

The first long-term ^{10}Be record published in 1981 is from an ice core from Dome C, Antarctica (Raisbeck et al., 1981b). This record covers 30 ka BP and shows a potential increase in the production rate inferred from relatively high ^{10}Be concentrations [atoms/g ice] during the Maunder Grand Solar Minimum. This is evidence of the link between ^{10}Be concentrations in ice cores and solar activity and, therefore, has shown the potential of ice core ^{10}Be to reconstruct long-term solar activity. Since then, long-term solar activity has been reconstructed from ice core ^{10}Be data from Greenland and Antarctica (e.g. Adolphi et al., 2014; Steinhilber et al., 2012; Vonmoos et al., 2006) bringing new knowledge about past solar activity beyond the instrumental era. Today's solar activity has been shown to be within the range of the Holocene solar activity in terms of magnitude and variation (Vonmoos et al., 2006). In additional, many important features of solar variability such as the 11-year cycle, the Gleissberg 88-year cycle (Gleissberg, 1965; Gleissberg & Schove, 1958) and the Suess or de Vries 207-year cycle (Damon & Sonett, 1991; Sonett & Suess, 1984) have been revealed and confirmed. There are also possibilities of solar variability on longer timescale such as 350-year (Knudsen et al., 2009; Steinhilber et al., 2012), 1000-year (Steinhilber et al., 2012), 1500-year (Bond et al., 2001) and the Hallstatt 2300-year (Damon & Sonett, 1991; Steinhilber et al., 2012; Usoskin et al., 2016) periodicities. However, the millennial-scale variations of solar activity are still unclear since the signals are weak and there are potential influences of uncorrected geomagnetic field variability on millennial-scale (Dergachev & Vasiliev, 2019).

One the other hand, ice core ^{10}Be is susceptible to climate influences from transport and deposition processes (Field et al., 2006; Heikkilä et al., 2009, 2014; Heikkilä & Smith, 2013; Pedro et al., 2006, 2011, 2012). The ^{10}Be concentrations from Dome C show an increase of ^{10}Be during the last ice age (30 – 15 ka BP) which indicates a climatic influence (Raisbeck et al., 1981b). High ^{10}Be concentrations during the last ice age were also found in the Camp Century ice core, Greenland (Beer et al., 1988). This record was compared with ^{14}C data from tree rings and both suggested possible long-term changes in the production rates, i.e. being 20% higher during the glaciation. However, no clear conclusion regarding solar activity could be made since strong climatic influences were clearly visible in the ^{10}Be record during the period. Later studies with the Greenland Ice Core Project (GRIP) and the Greenland Ice Sheet Project 2 (GISP2) ice core data proposed that the changes in ^{10}Be concentration during the transition from the ice age to the Holocene were mainly due to the dilution effect caused by changes in the snow accumulation rate (Finkel & Nishiizumi, 1997; Wagner et al., 2001; Yiou et al., 1997). Therefore, the high concentration of ^{10}Be during the ice age found in the previous studies could be mainly due to the lower precipitation rates during the ice age. A method to correct for this climatic effect is to calculate the ^{10}Be flux [atoms/cm^2.year], i.e. the product of the ice concentration and the snow accumulation rate (in term of ice equivalent) and ice density (~0.917 g/cm^3) (Finkel & Nishiizumi, 1997; Yiou et al., 1997). The calculated ^{10}Be fluxes from the GRIP and GISP2 ice cores show a high degree of similarity with the ^{14}C data from tree rings (after correcting for the effects of the carbon cycle) for the last 10 ka (Finkel & Nishiizumi, 1997; Muscheler et al., 2004). Nevertheless, millennial-scale changes in the two radionuclide records significantly deviated prior to 3 ka BP especially during the early Holocene (Vonmoos et al., 2006). Figure 2.6 shows that the ^{14}C production rate was systematically lower than the ^{10}Be fluxes before 3 ka BP which indicates a generally higher solar modulation inferred from the ^{14}C record. This difference can be attributed to uncorrected changes in the global carbon cycle. Moreover, the ^{10}Be flux is also not entirely free of climate signals (Field et al., 2006; Heikkilä et al., 2014; Heikkilä & Smith, 2013; Pedro et al., 2012). Overall, the exact cause for the deviation between ^{14}C and ^{10}Be records could not be pinpointed with the present knowledge and evidence.

Presently, only three long-term ^{10}Be records have been regularly used to reconstruct the Holocene solar activity. They are the GRIP and GISP2 ^{10}Be records from Greenland (Finkel & Nishiizumi, 1997; Vonmoos et al., 2006) and the EPICA Dronning Maud Land project (EDML) ^{10}Be record from Antarctica (Steinhilber et al., 2012). None of those records is continuously covering the complete Holocene epoch. They all have either gaps or end at ~9.4 ka BP. Moreover, the records do not cover the instrumental era (i.e. after the 1900s) due to missing of the top part in deep ice core drillings which makes the connection to the present ^{10}Be production rate challenging. A usual workaround is to combine the long-term ^{10}Be records with short-term ^{10}Be records (i.e. couple of hundreds to a thousand years) that cover the instrumental era (e.g. Steinhilber et al., 2012; Vonmoos et al., 2006). However, the differences between the sites of the long-term and short-term ^{10}Be records constitute another source of uncertainty for the Holocene solar reconstructions. For example, significant discrepancies were found between Greenland and Antarctic ^{10}Be records over the past 100 years (Muscheler et al., 2016; Zheng et al., 2021a) which illustrate the differences and local changes in

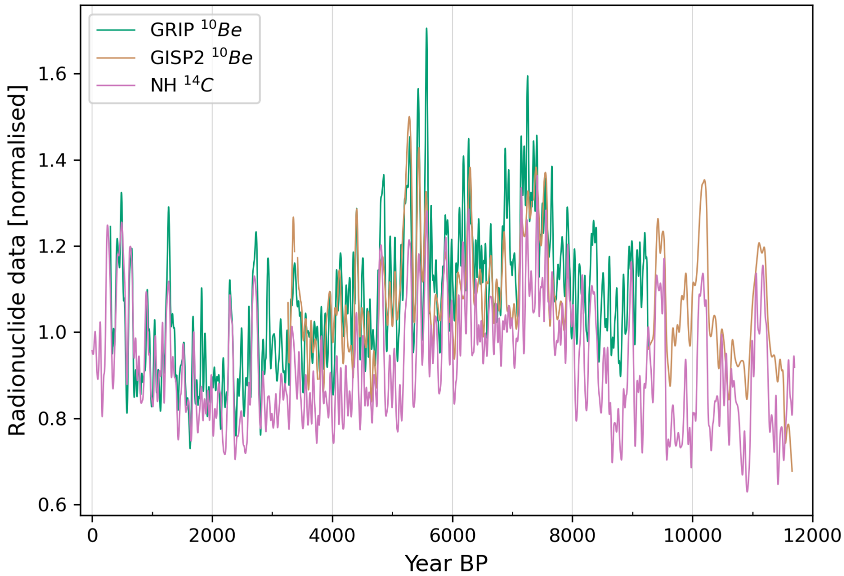

Figure 2.6: A comparison between the ^{10}Be fluxes from GRIP and GISP2 (Finkel & Nishiizumi, 1997; Vonmoos et al., 2006) and the ^{14}C production rate inferred from IntCal20 (Reimer et al., 2020). The data was interpolated to biannual resolution and then smoothed with a 26-year running mean filter to remove short-term variations. The GRIP ^{10}Be flux and ^{14}C data were normalised to have mean of 1 for the last 1 ka following Vonmoss et al., (2006). The GISP2 ^{10}Be flux was normalised to have the same mean with the GRIP ^{10}Be flux over their overlapping periods. Noted that the detail of the ^{14}C inference method can be found later in section 3.1.3 or in the supplementary information of paper 3.

the transport/deposition processes (Pedro et al., 2011). This thesis has been motivated by these challenges. A reliable solar activity reconstruction based on a new high quality and continuous record was deemed highly valuable for a complete and improved Holocene solar reconstruction. The preferred location is a dry site in Antarctica with low snow accumulation rates, dust input and a predominance of dry deposition to help reduce the local climate influences (Bard et al., 1997; Horiuchi et al., 2008). Such a record can help to improve our understanding of the current discrepancies between Greenland and Antarctica ^{10}Be and between ^{10}Be and ^{14}C.

In addition to the climatic effects, long-term influences of the GDM have been observed in the ^{10}Be records from ice cores. A period of lower ^{10}Be concentrations in the GRIP ice core can be observed around the geomagnetic field maximum at 2 ka BP (Muscheler et al., 2005). The Laschamps geomagnetic excursion that caused minimum shielding around 41 ka BP can also be observed in all Antarctic and Greenland ice cores as a period of enhanced ^{10}Be concentrations and fluxes (Muscheler et al., 2005; Raisbeck et al., 1987, 2017; Yiou et al., 1997). The event has been used to synchronize ice core records from the two polar regions (Raisbeck et al., 2017). In general, short-term variations in the ^{10}Be records from decadal (e.g. 11 years) to centennial (e.g. 88 years and 207 years) timescales can be attributed to solar activity while millennial-scale variations are believed to be due to GDM influences (Muscheler et al., 2005). Therefore, in some cases removal of millennial-scale variability from the ^{10}Be records using a hard frequency cut-off (i.e. a high-pass frequency filter) has been employed to minimise the GDM influence on the resulting solar activity estimate (Adolphi et al., 2014; Adolphi & Muscheler, 2016; Wagner et al., 2001). However, the Sun can possibly have variations on millennial-scales (Bond et al., 2001; Steinhilber et al., 2012; Usoskin et al., 2016) and also the GDM can vary on centennial-scales (Constable & Korte, 2015; Korte & Muscheler, 2012; Snowball & Muscheler, 2007). The GDM influence can therefore be, in theory, more reliably removed by using an independent dataset via an established relationship with the production rate (figure 2.5). Unfortunately, this transfers the uncertainties of the geomagnetic field data directly to the solar reconstruction. One might expect that the GDM should be one of the best constrained parts of the geomagnetic field, because of the large spatial scale. However, for various reasons, it is one of the geomagnetic field components where different models disagree the most (Panovska et al., 2015).

Reconstructions of solar activity often employ Monte Carlo sampling methods to account for the uncertainties in the geomagnetic field data (e.g. Vonmoos et al., 2006). This involves repeatedly and randomly selecting GDM values within the uncertainties at each point in time. However, such a method is purely numerical and often neglects the autocorrelation of the GDM on short timescale. The sampling process can go from a minimum value in one year to a maximum value in the next year which corresponds to unrealistically rapid changes in the GDM (Vonmoos et al., 2006). Consequently, this widens the error band of the solar reconstructions. A better method is to sample the whole curve (i.e. one possible realisation) generated from palaeomagnetic field models and through that the method accounts for the variation characteristics of the GDM (Adolphi & Muscheler, 2016). Unfortunately, this method could not reduce the unknown geomagnetic field uncertainties (i.e. dependences on which model you select) caused by the disagreements between the palaeomagnetic field models (e.g. figure 2.4). On the other hand, the solar reconstruction uncertainty could be further reduced if one can also account for the characteristic variations of solar activity. This could diminish the misinterpretation caused by noise in the radionuclide data that is not related to solar or geomagnetic modulation.

In summary, a better understanding of climate influences achieved via climate modelling and/or new and improved ^{10}Be records is important for the Holocene solar reconstructions. Millennial-scale reconstructions also require better constraints of the geomagnetic field influence. Finally, a better reconstruction/disentangling method is needed to account for the uncertainties induced by other sources than the Sun and the geomagnetic field.

2.4 Measurement of ^{10}Be in ice cores

Natural samples (e.g. rocks, sediments or ice core) contain only a minute amount of ^{10}Be leading to a typically low ratio of $^{10}Be/^{9}Be$ in the range from 10^{-7} to 10^{-11} (Christl et al., 2010; Lachner et al., 2020). Moreover, an additional amount of ^{9}Be is usually added for sample handling and measuring which further dilutes the ratio to 10^{-12} – 10^{-15}. This $^{10}Be/^{9}Be$ ratio is often several orders below the detection limit of conventional mass spectrometers (Beer et al., 2012). It should be noted that the isotopic ratio is usually measured since this is much easier in practice than counting the absolute number of a nuclide. Accelerator mass spectrometry (AMS) invented in the late 1970s was a ground-breaking technique in the field. In an AMS facility the ions are accelerated to very high kinetic energies before entering the mass spectrometer which allows for more efficiently differentiation against the background noise (i.e. species with the same molecule mass (isobars) and other much more abundant stable isotopes or molecules) (Beer et al., 2012; Kutschera, 2013; Raisbeck et al., 1978). This strongly reduces the background noise and lowers the detection limit by many orders of magnitude compared to a conventional mass spectrometry (Kutschera, 2013; Synal, 2013) which allows for the measurement of ^{10}Be.

The isotopic $^{10}Be/^{9}Be$ ratio in ice cores can only be measured via AMS if a small amount of ^{9}Be, the so-called carrier, is added before melting the ice samples. The reason is that ^{9}Be cannot be found in the atmosphere except for in dust grains (Beer et al., 2012) and therefore extremely low quantities of ^{9}Be are deposited onto the Greenland and Antarctic ice sheets. The amount of ^{9}Be carrier added to a sample usually varies from 0.1 to 0.3 mg (e.g. Adolphi et al., 2014; Aldahan, 1998; Horiuchi et al., 2007; Raisbeck et al., 1987, 2006, 2007; Yiou et al., 1997) depending on the expected amount of ^{10}Be atoms. In a typical process an ice core ^{10}Be sample is melted together with a defined amount of ^{9}Be carrier and the sample is then passed through an ion exchange column (IEC) that retains Be while removing the excess melt water. Be^{2+} binding to the IEC is extracted with HCl. In the next step, the eluted Be is precipitated as $Be(OH)_2$ via raising the solution pH with NH_4OH. Afterward, $Be(OH)_2$ is oxidized to BeO via heating at high temperature (800 – 900ºC). A common extra step prior to the heating process is to wash the precipitated $Be(OH)_2$ with purified water (Raisbeck et al., 2007) mainly to remove NH_4Cl which can sublimate at ~340ºC and potentially contaminate the sample and the heating system. Finally, the AMS measurement is conducted on the BeO^- ion.

3 Material and Methods

3.1 The ^{10}Be record from Little Dome C

3.1.1 Sample description

The new Holocene ^{10}Be record presented in this thesis comes from a site called Little Dome C (LDC, 75.36ºS and 122.42ºE) around 40 km away from the Dome Concordia (Dome C) station (figure 3.1). This LDC site has a low snow accumulation rate of ~2 cm/year which is slightly lower than at the neighbouring Dome C site. The ice samples were retrieved by the British Antarctic Survey during their second drilling campaign at LDC in the austral summer of 2017/18. The purpose of the campaign was to perform site survey drillings for the Beyond EPICA - Oldest Ice project, i.e. to identify a potential drill site to recover ice older than 1.5 Ma (Lilien et al., 2021; Rowell et al., 2022). A new drilling technique, so-called Rapid Access Isotope Drill, was employed to quickly retrieve the ice (in the form of ice chips) and perform preliminary measurements such as water isotopic composition (Rix et al., 2019). A 462 m deep drilling was performed in just over 104 hours during the campaign.

In total, 1056 samples of ice chips that continuously cover the entire depth are available for ^{10}Be measurements. These samples are estimated to cover the last ~20 ka. Each of the sample covers a depth ranging from 1.6 to 79.2 cm with an average of 43.6 cm. There is potential mixing during the drilling and sample handling (e.g. dividing the ice chips into samples bears the risk that they were mixed up during drilling in contrast to an intact ice core where samples could be divided by perfect cuts). This could lead to some degree of smoothening in the measurement results which should be evaluated.

3.1.2 Measurement of the samples

Over the course of this PhD project, 759 ^{10}Be samples covering 332 m depth were measured. The samples were prepared at the 10Be Lab of the Department of Geology of Lund University (Sweden) and were then measured at the 300 kV MILEA facility of the Laboratory of Ion Beam Physics at ETH Zurich (Switzerland). The sample preparation process for accelerator mass spectrometry (AMS) measurement was conducted using an optimised procedure that was investigated in paper number 1 (Nguyen et al., 2021). The procedure can be summarised as follow:

1) ~45 g of ice is extracted from each original sample.
2) 0.15 mg ^{9}Be carrier is added directly to the ice and they are melted together in a microwave
3) 0.15 mg of Fe and 2 mL of NH_3 solution (25%) are added to raise the pH of the melted solution. $Be(OH)_2$ is co-precipitated with $Fe(OH)_3$ overnight resulting in reddish-brown gel.
4) The sample is centrifuged to separate the gel from the liquid part which is discarded.
5) The gel is then oxidised from $Be(OH)_2$ to BeO through a three-step heating process:
   - Heating at 150ºC for 2 hours

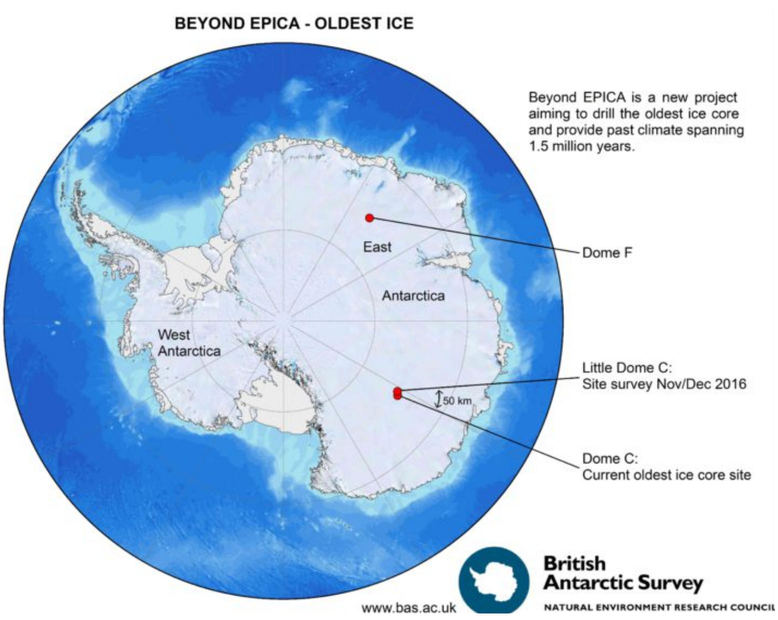

Figure 3.1: Drilling sites of the Beyond Epica – Oldest Ice project. *Credit: British Antarctica Survey*

- The temperature increases from 150 to 850ºC within 2 hours
- Heating at 850ºC for another 2 hours

6) The oxidised sample is mixed with ~1 mg of Nb-powder then then pressed into an AMS target holder which is then sent to ETH Zurich for measurement.

In comparison to the regular preparation procedure discussed in section 2.4, we have eliminated the Ion Exchange columns (IECs) and the washing process of the precipitate $Be(OH)_2$ before heating (Raisbeck et al., 2007). These two steps are unnecessary for the LDC samples and risk introducing noise to the AMS measurement (Nguyen et al., 2021). In addition, we also co-precipitate our sample with Fe since this leads to more consistent AMS measurement. Figure 3.2 illustrates the six main steps in our procedures with pictures.

3.1.3 Timescale of the Little Dome C samples

The LDC timescale was initially estimated based on the depth-to-age relationship of the nearby Epica Dome C (EDC) ice core (Veres et al., 2013). This is a reasonable first-order estimation due to the close proximity and shared climate features between LDC and Dome C. However, Rowell et al. (2022) showed a shift in the age-to-depth relationship toward older ages at LDC via comparing the deuterium records (Figure 3.3) between the two sites which is expected due to the lower accumulation rate at LDC. The LDC ice tends to be older than the EDC ice at the same depth and the difference is more significant with lower depth. The large increase in the deuterium records due to the transition from a cold glacial climate to a warm Holocene climate occur earlier (at shallower depth) in LDC. Therefore, the age-to-depth relationship of LDC was stretched by 8% to get the best fit between the deuterium records in the two sites.

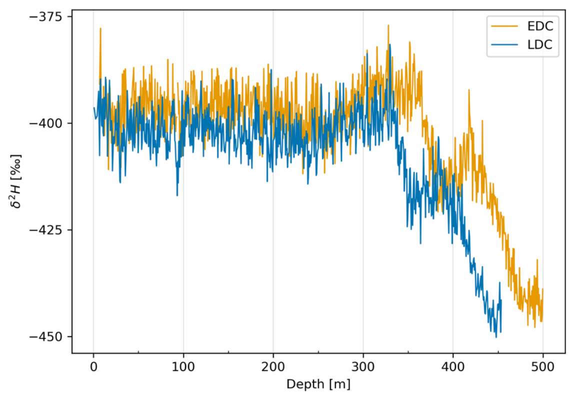

Figure 3.3: A comparison of the EDC deuterium record (Stenni et al., 2010) and the LDC deuterium record (Rowell et al., 2022). Replotted from Rowell et al. (2022).

The initial timescale derived from the stretched age-to-depth relationship was then synchronised to the IntCal20 timescale (Reimer et al., 2020) using a Bayesian wiggle-matching method (Adolphi & Muscheler, 2016). The basics for this method are that

Figure 3.2: Six main steps in the preparing procedure of ^{10}Be sample at Lund University for AMS measurement. (1) A sample of ice chip from LDC, (2) after the addition of the ^{9}Be carrier the sample is melted using a microwave, (3) $Be(OH)_2$ and $Fe(OH)_3$ precipitate in the bottom of the tube in the form of reddish-brown gel, (4) the gel is separated from the liquid part via centrifugation, (5) the samples are heated during our three-step heating with a special oven and (6) an AMS target.

^{10}Be and ^{14}C share similar variations at centennial-scales between 150 to 500 years (Adolphi et al., 2014; Adolphi & Muscheler, 2016). First, we inferred the global ^{14}C production rate from the IntCal20 Northern Hemisphere calibration curve. The calibration curve was compiled by the IntCal Working Group for improving the ^{14}C age calibration and it can be used to reconstruct fluctuations in past atmospheric ^{14}C concentrations. We employed a box diffusion carbon model that consists of atmosphere, biosphere, upper ocean mixed layer and 42 deep-sea layers (Siegenthaler, 1983). The option for direct ventilation of the deep ocean was turned off, and the surge in atmospheric CO_2 from 1850 CE due to fossil-fuel burning was included in the calculation to account for the dilution of ^{14}C in relation to ^{12}C. This inference method has been repeatedly conducted based on the previous version of IntCal (Adolphi et al., 2014; Adolphi & Muscheler, 2016; Knudsen et al., 2009; Korte & Muscheler, 2012; Muscheler et al., 2004, 2005). The variations between 150- to 500-year timescale of ^{14}C and LDC ^{10}Be were extracted via computing a normalised production rate following Muscheler and Heikkilä (2011):

$$Q_{norm} = \frac{Q_{lp150}}{Q_{lp500}} \quad (3.1)$$

where Q_{lp150} and Q_{lp500} are the low-pass filtered production rates with cut-off frequencies of 1/150 year^{-1} and 1/500 year^{-1}, respectively. Q_{norm} is the normalised production rate showing only variations between 150- to 500-year timescale. The normalised ^{10}Be record is divided into windows of 1000 years and then each window is synchronised/compared with the normalised ^{14}C production rate. The process results in a timescale transfer function from the LDC timescale to the IntCal20 timescale (figure 3.4). Further details of the Bayesian wiggle-matching method and the inference method of ^{14}C production rate from IntCal calibration curve can be found in Adolphi & Muscheler (2016).

3.1.4 Past accumulation rate reconstruction

Reconstruction of ^{10}Be flux from the ^{10}Be concentration measured with AMS requires information on past snow accumulation rates at LDC. The past accumulation rate can be reconstructed via modelling the ice flow (e.g. Parrenin et al., 2007) but this modelling process is often complicated and requires a lot of resources. Since we already have the depth-to-age relationship, the accumulation rate at LDC can be derived using the following formula:

$$dz/dt = A * T(z) \quad (3.2)$$

where dz/dt [m/year] denotes the thickness of an ice layer accumulated over a period of time. This term can be inferred from the depth-to-age relationship. A is the past accumulation rate [m of ice equivalent/year]. $T(z)$ is the thinning function indicating the vertical compression of the ice layer with values ranging from 0 to 1. It could also be understood that A is the initial layer thickness of the ice and $T(z)$ is the compression factor accounting for the ice flow. We adopted the

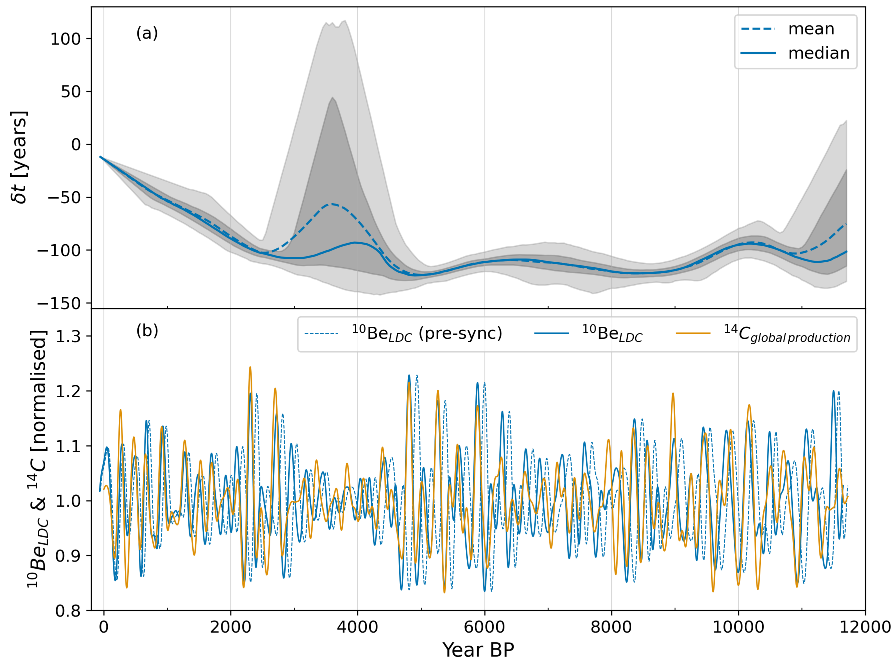

Figure 3.4: (a) Timescale transfer function with envelopes of 50% CI (dark grey) and 95% CI (light grey). δt indicates the age difference between $t_{IntCal20}$ and t_{LDC}, i.e. $t_{IntCal20} - t_{LDC}$. (b) A comparison of the variations at timescales between 150 – 500 years of LDC ^{10}Be and ^{14}C production rate before and after the synchronisation. Noted that the LDC timescale before the synchronisation is based on the EDC age-to-depth relationship (Veres et al., 2013) stretched by 8% (see text).

thinning function of EDC (Veres et al., 2013) based on the observation that the LDC and EDC sites share similar climate features and so the thinning function of LDC should, similar to the thinning function of EDC, change very little above 400 m depth. Indeed, the EDC thinning function gradually decreases from 1 at the surface to 0.92 at 400 m depth.

3.2 A novel Bayesian model to reconstruction solar activity

Paper number 2 (Nguyen et al., 2022) is dedicated to presenting the Bayesian model which includes outlining the framework, parameterisation and testing of the model. Therefore, this section gives only a brief summary of the model's concept. Recent geomagnetic field models have successfully adopted a Bayesian inference approach where model parameters are considered jointly distributed and so their probability distribution can be estimated using Markov Chain Monte Carlo (MCMC) methods (Hellio & Gillet, 2018; Nilsson & Suttie, 2021). Inspired by these approaches, we have also adopted the Bayesian approach to disentangle solar and geomagnetic field influences from the radionuclide records. We model the global production rate of cosmogenic radionuclides (Q) using the established relationship (figure 2.5) with the solar modulation potential (ϕ) and the GDM (M). ϕ and M are considered as jointly distributed parameters of this model and so their probability distribution can be estimated accordingly to the Bayes' theorem (Gelman et al., 2004):

$$p(\phi, M|Q) \propto p(Q|\phi, M) * p(\phi, M) \quad (3.3)$$

If ϕ and M are independent, the formula can be re-written as:

$$p(\phi, M|Q) \propto p(Q|\phi, M) * p(\phi) * p(M) \quad (3.4)$$

where $p(\phi)$ and $p(M)$ are the prior distribution of the parameters. $p(Q|\phi, M)$ can be treated as the likelihood function, i.e. a function with parameters ϕ and M. $p(\phi, M|Q)$ is the posterior distribution of the parameters considering the observed production rate Q. The joint posterior distribution of ϕ and M is estimated using MCMC methods via the following workflow:

1) The model generates a random set of parameters ϕ and M based on their prior distribution.
2) A corresponding production rate is computed from the generated set of parameters using the likelihood function.
3) The model evaluates this proposed production rate (also via the likelihood function) with the observed production rate and the observation uncertainty and then it decides to reject or accept the set of ϕ and M.

The likelihood function is given as:

$$Q \sim N(f(\phi, M), \sigma_Q^2) \quad (3.5)$$

where $f(\phi, M)$ is the established relationship between ϕ, M and Q. σ_Q^2 represents the observation uncertainty. This MCMC process keeps on going until a certain number of sets of ϕ and M are accepted (N = 1000 in our case). These 1000 sets are used to estimate of the posterior probability distribution of ϕ and M. The model was built and executed in Stan, a probabilistic programming language for statistical modelling and high-performance statistical computation (Carpenter et al., 2017).

The Bayesian model gives us the opportunity to incorporate the characteristic variations of solar activity and GDM into the reconstruction process via parameterisation of their prior distribution $p(\phi)$ and $p(M)$. As discussed in section 2.3.2, utilising the characteristic variations can reduce the noise and reconstruction uncertainty. Moreover, this modelling approach can reconstruct solar activity and GDM at the same time via disentangling their influences on the radionuclide data. Only information on the characteristic variations of GDM is required here instead of completely independent reconstructions. Therefore, the model also minimises the uncertainty associated with the independent GDM reconstructions including the present discrepancies between them. On the other hand, the independent GDM reconstructions can be used to evaluate the model reconstruction which is an extra independent validation for the radionuclide-based solar and GDM reconstructions.

Parameterisation of the prior distribution is an important step that requires reliable information on solar and GDM variations. We used the information extracted from the Group Sunspot number (GSN) record (Svalgaard & Schatten, 2016), since this is the longest direct observation record (~400 years) that is not influenced by the Earth's climate and the GDM. The drawback is that, due to the short time span, the GSN record only contains decadal up to 200-year timescale variations. This leads to less certainty in the reconstruction of longer centennial-scale variations and possible millennial-scale variations. However, information on longer timescales of solar variability can only be extracted from cosmogenic radionuclide records and we want to avoid circular reasoning as the model is intended to be applied to the radionuclide records. On the other hand, the prior distribution of GDM is parameterised similarly as a recent Holocene geomagnetic model, the so-called pfm9k.2 model (Nilsson et al., 2022). We simplify the geomagnetic modelling and use only the axial dipole component to approximate the GDM since this component dominates the geomagnetic shielding of GCRs (Masarik & Beer, 1999).

4 Summary of papers

This thesis is compiled of three papers that aim at (1) discussing the new Little Dome C (LDC) ^{10}Be record, (2) introducing a new Bayesian model to reconstruct solar activity, and (3) utilising the new data and method to deliver a most up-to-date and complete Holocene solar reconstruction. Contributions of the authors to each paper are shown in table 1.

4.1 Paper I

Nguyen, L., Paleari, C., Müller, S., Christl, M., Mekhaldi, F., Gautschi, P., Mulvaney, R., Rix, J., Muscheler, R., 2021. The potential for a continuous 10Be record measured on ice chips from a borehole. Results in Geochemistry 5, 100012, doi: 10.1016/j.ringeo.2021.100012.

Paper 1 aims at (1) introducing the new LDC ^{10}Be record, (2) optimising the sample preparation method for accelerator mass spectrometry (AMS) measurement and (3) evaluating the potential of the record for solar reconstruction. The sample preparation method was tested and optimised based on surface ice chips also from LDC, snow collected in Lund (Sweden) and frozen Milli-Q water. The results show that some of the regular steps in the preparation process are not necessary for our samples including filtering of the melted ice samples with Ion Exchange Columns (IECs) and washing the precipitate of $Be(OH)_2$ with Milli-Q water before heating. Meanwhile, co-precipitating Be with Fe would lead to more consistent AMS measurement. The optimised preparation method was applied to the 76 uppermost samples from LDC (1354 – 1950 CE). The ^{10}Be concentrations resulting from AMS measurements agree well with ^{10}Be concentrations from the South Pole ice core in central Antarctica (Raisbeck et al., 1990) and the global ^{14}C production rate inferred from IntCal20 (Reimer et al., 2020). The LDC ^{10}Be concentrations also reflect the solar signal including the Spörer Minimum (1460 – 1550 CE) and the Maunder Minimum (1645 – 1715 CE). This result indicates the potential of LDC ^{10}Be for solar reconstruction. We also evaluated the possible mixing of ice chips during the process of drilling and sample handling (e.g. dividing the samples) and found, through comparison to independent data, insignificant mixing between the samples.

4.2 Paper II

Nguyen, L., Suttie, N., Nilsson, A., Muscheler, R., 2022. A novel Bayesian approach for disentangling solar and geomagnetic field influences on the radionuclide production rates. Earth, Planets and Space 74, 130, doi: 10.1186/s40623-022-01688-1.

Paper 2 aims at presenting a new Bayesian model that has been developed for the reconstruction of solar activity and of the geomagnetic dipole moment (GDM) from the radionuclide records. We employed a Bayesian inference approach where solar activity and GDM are treated as jointly distributed parameters of the radionuclide production rate. This allows us to estimate their probability distribution using Markov Chain Monte Carlo (MCMC) methods. We used a ~2000 years record of ^{14}C production rate (1 – 1950 CE) inferred from IntCal20 (Reimer et al., 2020) to evaluate and apply the model. Model testing and evaluation were conducted on synthetic data corrupted with realistic noise. After the synthetic test has indicated that the model performs well, we applied it to the ^{14}C data to reconstruct solar activity and GDM for the last two millennia. Our solar reconstruction shows similar short-term variations as the group sunspot number (GSN) record (Svalgaard & Schatten, 2016) with some minor differences in the long-term variation around 1700 – 1800 CE. Our GDM reconstruction mostly agrees with independent geomagnetic field models (Hellio & Gillet, 2018; Nilsson et al., 2014). Our Bayesian model outperforms various frequency filters which have usually been employed to target and extract solar activity and GDM variations from the radionuclide records at a specific timescale range (Adolphi et al., 2014; Muscheler et al., 2005; Snowball & Muscheler, 2007; Zheng et al., 2021b). In conclusion, the model is very useful for disentangling solar and GDM influences from the radionuclide data, and there is potential for further development via including additional confounding factors such as climate and carbon influences on the radionuclide records.

4.3 Paper III

Nguyen, L., Suttie, N., Nilsson, A., Müller, S., Christl, M., Gautschi, P., Mulvaney, R., Rix, J., Muscheler, R.,. No evidence for multi-millennial scale variations of solar activity during the Holocene constrained from cosmogenic radionuclides. (Manuscript)

Paper 3 aims to apply the Bayesian model on the new LDC ^{10}Be record, other previous long-term ^{10}Be records and the ^{14}C production rate to provide a complete Holocene solar activity reconstruction. The previous long-term ^{10}Be records are from the EPICA Dronning Maud Land project (EDML, Steinhilber et al., 2012) and the Western Antarctic Ice Sheet (WAIS, Sigl et al., 2016) ice cores in Antarctica, and from the Greenland Ice Core Project (GRIP, Vonmoos et al., 2006) and the Greenland Ice Sheet Project 2 (GISP2,

Table 1: Author contributions to the three papers in this thesis compilation

	Paper I	Paper II	Paper III
Study design	L. Nguyen C. Paleari S. Müller M. Christl F. Mekhaldi R. Muscheler	All authors	L. Nguyen N. Suttie A. Nilsson R. Muscheler
Data/Sample collection	S. Müller R. Mulvaney J. Rix R. Muscheler	A. Nilsson R. Muscheler	L. Nguyen A. Nilsson R. Mulvaney J. Rix R. Muscheler
Sample preparation	L. Nguyen C. Paleari S. Müller	-	L. Nguyen S. Müller
Sample measurement	M. Christl P. Gaustchi	-	M. Christl P. Gaustchi
Data analysis and/or modelling	L. Nguyen M. Christl	L. Nguyen A. Nilsson	L. Nguyen
Data interpretation and discussion	L. Nguyen C. Paleari S. Müller M. Christl F. Mekhaldi R. Muscheler	All authors	L. Nguyen N. Suttie A. Nilsson R. Muscheler
Writing first draft	L. Nguyen	L. Nguyen	L. Nguyen
Writing: Commenting, reviewing and editing	All co-authors	All co-authors	All co-authors

Finkel & Nishiizumi, 1997) ice cores in Greenland. We evaluated the quality of the ^{10}Be records via comparing the ^{10}Be concentrations and fluxes to estimate the influence of snow accumulation changes. While good agreements between the ^{10}Be concentration and fluxes are found for the LDC and GRIP records, systematic differences due to climate influences can be observed at EDML, WAIS and GISP2. The systematic differences at WAIS and GISP2 are too significant for any reliable reconstructions. Therefore, we excluded them and applied the Bayesian model on the ^{10}Be concentration records of LDC, EDML and GRIP and the ^{14}C production rate. The results show persistent solar activity from decadal up to 350-year timescales throughout the Holocene. We also found hints of a solar cycle around 1000-year length. Variations on timescales longer than 1000 years are, however, inconsistent between the records. In addition, the amplitude of the centennial variations appears to change on millennial-scales. The variations were relatively weak during the periods from around 2 to 1 ka BP, 4.5 to 3 ka BP and 8 to 6.4 ka BP and have been strong otherwise. This bundling of strong centennial-scale variations followed by periods of weaker centennial-scale variability are most likely the source of the weak millennial-scale variations. We also evaluated the model results with the independent GDMs based on paleomagnetic data and found that long-term (multi-millennial) differences between the records that are reflected in the reconstructed GDMs. Since the differences are not systematic (i.e. in the same direction) we argue that these cannot be attributed to multi-millennial-scale solar activity variations that were misinterpreted as GDM variability by the Bayesian model. In conclusion, we found no solid evidence of multi-millennial solar variations over the Holocene periods.

5 Discussion

5.1 The Little Dome C ^{10}Be data quality

Figure 5.1 shows the accelerator mass spectrometry (AMS) measurement uncertainty of the ^{10}Be concentrations from Little Dome C (LDC). The average measurement uncertainty is 3.4 % with some exceptional measurements that exceed 8% uncertainty. This generally low measurement uncertainty can be attributed to improvements of the AMS system at ETH in recent years (Christl et al., 2013).

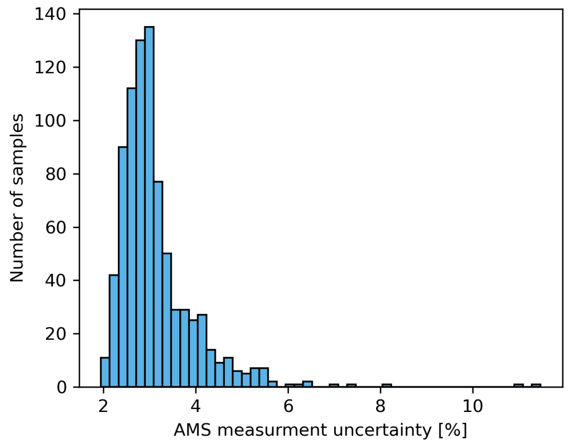

Figure 5.1: AMS measurement uncertainty distribution of the LDC ^{10}Be samples

Figure 3.4a shows the timescale transfer function for the LDC samples to the IntCal20 timescale (Reimer et al., 2020). It shows that the initial LDC timescale, that based on the Epica Dome C (EDC) age-to-depth relationship (Veres et al., 2013) stretched by 8%, generally overestimates the age of the samples. The average age difference (δt) between LDC and IntCal20 increases from 12 years during the recent period to 100 years at 4.3 ka BP and remains around that level for the rest of the Holocene period. The 1-σ uncertainty for the adjusted timescale is mostly within 10 years except for the periods between 5 to 2 ka BP and around the early Holocene (before 10.5 ka BP). The disagreements between centennial variations of ^{14}C and LDC ^{10}Be during those periods (figure 3.4b) resulted in a poor synchronisation between the ^{14}C and LDC ^{10}Be records and consequently a large 1-σ uncertainty of up to 85 years. The reason for the differences in the centennial-scale variations are not yet understood. However, the timescale transfer function could still be considered as reliable since the chronology of LDC is consistent without any erratic changes (compared to the IntCal20 timescale) before and after the disagreement periods. Moreover, large deviations in accumulation rates which can lead to erratic timescale variations are unlikely considering the history of accumulation rates at the adjacent EDC site (figure 5.2a).

Figure 5.2a shows the reconstructed accumulation rate at LDC compared to the EDC accumulation rate (Veres et al., 2013). The thinning function of the EDC ice core (Veres et al., 2013) was used together with the IntCal20 timescale to reconstruct the accumulation. The blue shading demonstrates the upper and lower boundaries of the LDC accumulation rate constrained by the accumulation rate and the thinning ratio (figure 5.2b) at EDC, respectively. The lower boundary of the accumulation rate is based on an extreme scenario of no ice-flow-related compression at LDC and so the value of the thinning function is constant at 1. The

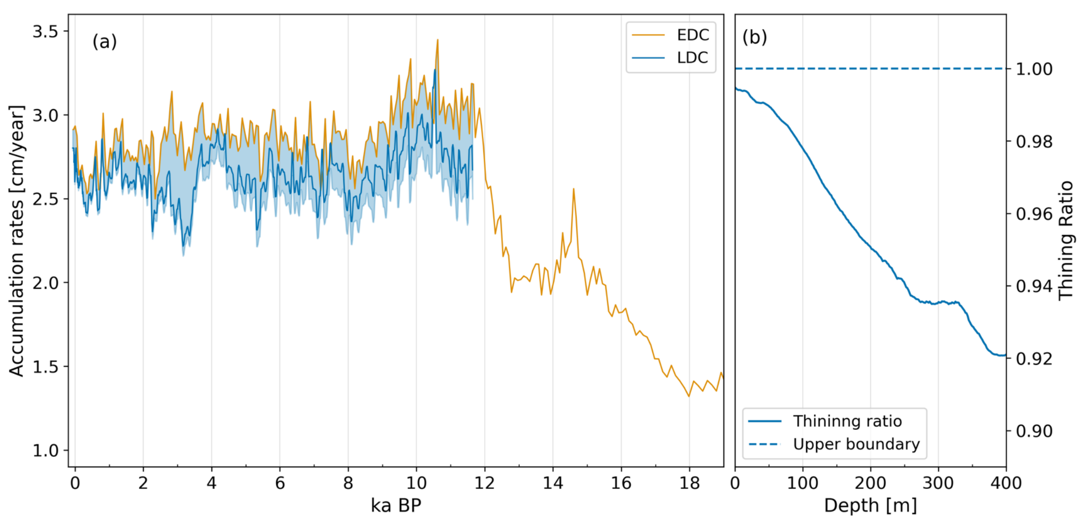

Figure 5.2: (a) Snow accumulation reconstruction at LDC compared to at EDC. The upper and lower boundaries of the LDC accumulation rate were constrained by the accumulation rate and the thinning ratio at EDC (Veres et al., 2013), respectively. (b) The EDC thinning ratio and its upper boundary.

upper boundary of the accumulation rate is based on the assumption that the past accumulation rate at LDC was equal or lower than at EDC. The low accumulation assumption at LDC is likely to hold true as due to the shift in the age-to-depth relationship (toward lower ages) from EDC to LDC discussed above. If the accumulation rate at LDC was significantly higher than at EDC, one would expect a more drastic decrease in the thinning ratio with lower depth (to compensate for the large accumulation rate). This is unlikely considering the proximity and the shared climate features of LDC and EDC sites (Rowell et al., 2022). Moreover, the good agreement of centennial- and millennial-scale variations between EDC and LDC accumulation rates (figure 5.2a) also supports our assumption. Another source of uncertainty for LDC accumulation reconstruction is the timescale transfer function. The transfer function can significantly affect the accumulation rate if there are strong short-term variations in the age difference between LDC and IntCal20. This will induce changes in the age differences between layers dt in equation 3.2 and consequently lead to changes in dz/dt that influence the reconstructed accumulation rate. However, since the age difference is mostly consistent between LDC and IntCal20 timescales (figure 3.4a) we expect little changes in dt and so insignificant effects on the reconstructed accumulation rate.

Figure 5.3 shows the ^{10}Be concentration and flux of LDC and the ^{10}Be concentrations and fluxes of the published long-term ^{10}Be records, i.e. the Greenland Ice Core Project (GRIP, Vonmoos et al., 2006), the Greenland Ice Sheet Project 2 (GISP2, Finkel & Nishiizumi, 1997), the EPICA Dronning Maud Land project (EDML, Steinhilber et al., 2012) and the Western Antarctic Ice Sheet ice core (WAIS, Sigl et al., 2016). The EDML, WAIS and GISP2 ^{10}Be fluxes were computed using their corresponding accumulation records (Cuffey et al., 1995; Cuffey & Clow, 1997; Fudge et al., 2016; Veres et al., 2013). All data has been interpolated into 2-year (biannual) resolution. The biannual data was then filtered with a 26-year running mean filter. This data processing was conducted to obtain records consistent with the published GRIP ^{10}Be record (Vonmoos et al., 2006). The LDC record was normalized to have a mean of 1 over the Holocene (data set divided by its own mean value). The other records were normalized to LDC so that they have the same mean during their overlapping periods.

^{10}Be concentrations and fluxes are the two end-members to estimate the atmospheric ^{10}Be concentration production rate (Alley, 1995) and their differences can indicate the potential climate influences on the ^{10}Be record. The ^{10}Be concentration and flux of LDC show similar trends over the

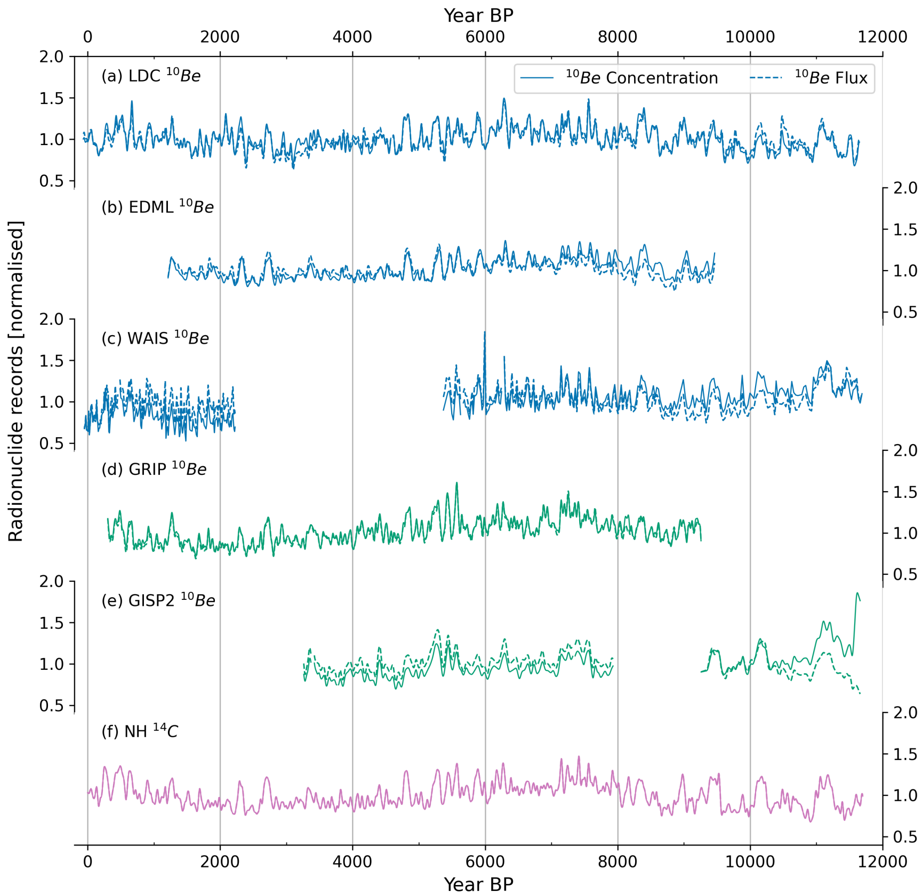

Figure 5.3: (a-e) ^{10}Be flux vs concentration of the long-term ^{10}Be records from Antarctica including LDC (this study), EDML (Steinhilber et al., 2012), WAIS (Sigl et al., 2016) and from Greenland including the GRIP (Vonmoos et al., 2006) and GISP2 (Finkel & Nishiizumi, 1997) ^{10}Be records. (f) ^{14}C production rate inferred from the IntCal20 Northern Hemisphere calibration curve (Reimer et al., 2020).

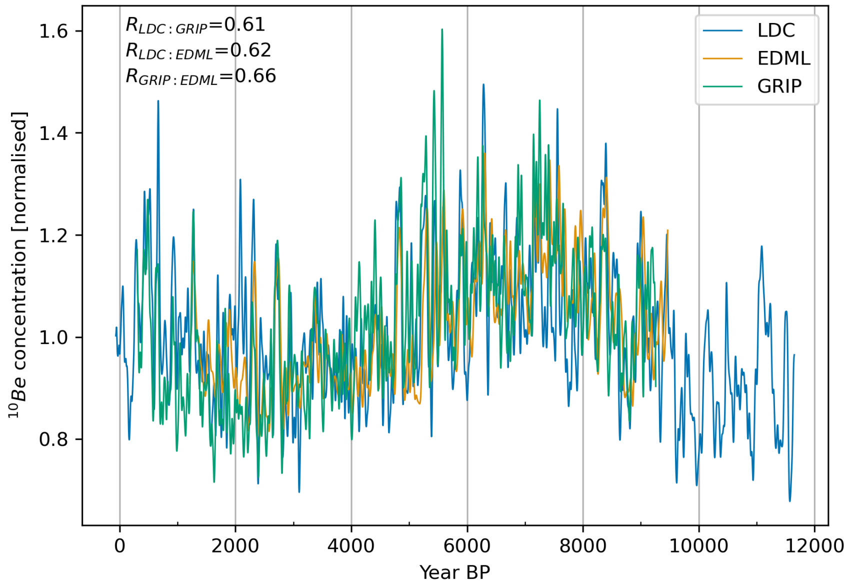

Figure 5.4: A comparison between ^{10}Be concentration from LDC, EDML and GRIP. The correlation coefficients are shown for the overlapping periods.

Holocene with only slight differences. The ^{10}Be flux from EDML was systematically higher than the concentrations before 6 ka BP and was lower than the concentrations after 5 ka BP. This difference in the long-term trend is caused by a gradual increase in the accumulation rate at EDML (Veres et al., 2013). A similar systematic difference is also present in the long-term trend between ^{10}Be concentration and flux of WAIS. In the GRIP ice core, a high degree of similarity between ^{10}Be concentration and flux can be observed. On the other hand, the ^{10}Be flux of GISP2 significantly deviated from the concentration in the early Holocene due to the sharp increase in accumulation rate during the period at the site (Cuffey et al., 1995; Cuffey & Clow, 1997). It should be mentioned that, the thinning function can change significantly due to different assumptions in the ice flow model which leads to different long-term trends in the accumulation rate. For example, there are three proposed scenarios of the marginal retreat of the ice sheet at GISP2 (i.e. 50 km, 100 km and 200 km; Here, we used the accumulation rate associated with the 100 km of marginal retreat scenario) that produce different thinning function curves and consequently different trends in the accumulation rate. The uncertainty associated with the thinning function can contribute partially or even considerably to the differences between the ^{10}Be concentrations and ^{10}Be fluxes at EDML, WAIS and GISP2. Overall, the ^{10}Be records of GRIP and LDC are likely the least influenced by the snow accumulation changes and therefore arguably better than the rest for estimating the atmospheric ^{10}Be concentration.

A major advantage of the LDC ^{10}Be record is the complete coverage of the entire Holocene. The ^{10}Be records from WAIS and GISP2 contain big gaps of more than 1000 years. This leads to missing information in their long-term trend and also difficulties in normalisation of the data. On the other hand, the GRIP and EDML ^{10}Be records lack data over the instrumental era (i.e. after the 1900s) in order to connect to the well constrained production rate. Combining the GRIP and EDML ^{10}Be data with recent short records (usually shorter than 1 ka) has been conducted (e.g. Steinhilber et al., 2012; Vonmoos et al., 2006) to overcome this problem. However, the noise and differences among the short records (Muscheler et al., 2016; Zheng et al., 2021a) constitute another source of uncertainty. In summary, the LDC ^{10}Be record exhibits none of the challenges and should help to improve the quality and coverage of a global ^{10}Be production rate estimate for the Holocene epoch.

5.2 Discrepancy between the long-term ^{10}Be records

Figure 5.4 shows LDC ^{10}Be concentration in comparison with the GRIP and EDML ^{10}Be concentrations. The GRIP and EDML^{10}Be records have been regularly used for Holocene solar reconstruction at the moment due to their continuousness and good temporal resolution. The records show similar variations before 3 ka BP except for a short period around 7.5 ka BP. During this period, the LDC record exhibited a sharp drop in the ^{10}Be concentrations by around 20% to 30% compared to the EDML and GRIP records. Differences between the three records can also be observed after 3 ka BP. The LDC ^{10}Be concentration experienced a gradual increasing trend, while the GRIP ^{10}Be concentration was 10% to 20% lower. The EDML ^{10}Be concentration was in between the LDC and GRIP ^{10}Be concentrations. Possible explanations for this long-term discrepancy are (1) changes in the transport of ^{10}Be to the sites, (2) changes in the deposition of ^{10}Be

at the sites (e.g. changes in the accumulation rate) and (3) a potential strong asymmetry occurred in the geomagnetic field during the period leading to different shielding effects between the Northern and Southern hemispheres. For the third explanation, the persistent north-south hemispheric asymmetry for the past few thousand years with generally lower field intensity in the southern hemisphere (Constable & Korte, 2015; Nilsson et al., 2022) could lead to an increase in ^{10}Be production rate that reflects in the higher ^{10}Be concentration in LDC and EDML (southern hemisphere) than in GRIP (northern hemisphere). However, there are also differences between the LDC and EDML during the period the third reason alone cannot fully explain for the discrepancies between the records. Overall, the unresolved long-term differences between the ^{10}Be records lead to uncertainties in the Holocene reconstructions, particularly for the last 3 ka.

5.3 Potential polar bias in the ^{10}Be record

Here, I evaluate the potential presence of the polar bias discussed in section 2.3.1 (i.e. the dominance of high latitude ^{10}Be in the ice core records, Adolphi et al., 2023; Bard et al., 1997; Field et al., 2006; Heikkilä et al., 2009; McCracken, 2004; Pedro et al., 2012; Steig et al., 1996). This bias enhances the signal of solar activity and dampens the GDM influence due to the low geomagnetic shielding in the polar regions. Figure 5.5 shows the geomagnetic dipole moment (GDM) based on ^{10}Be concentrations of LDC (GDM_{LDC}), EDML (GDM_{EDML}) and GRIP (GDM_{GRIP}) in comparison to independent GDM reconstructions based on paleomagnetic data (e.g. lake and marine sediments, volcanic rocks and archaeological materials) (Constable et al., 2016; Knudsen et al., 2008; Nilsson et al., 2022; Pavón-Carrasco et al., 2014). The GDM reconstructions from the ^{10}Be records were conducted using the Bayesian method (Nguyen et al., 2022 and paper number 3). Here, we focus on discussing the polar bias effect in the ^{10}Be records which should reduce the variations of the reconstructed GDMs. The discrepancies between the reconstruction are discussed in detail in paper number 3.

GDM_{GRIP} shows a similar degree of variations as the independent GDMs. Although GDM_{EDML} shows a different long-term trend for the period after 4 ka BP, the values of GDM_{EDML} were in the same ranges as the independent GDMs before 4 ka BP. This suggests a somewhat similar degree of variations between GDM_{EDML} and the independent GDMs during this earlier period. On the other hand, the variations of GDM_{LDC} are clearly suppressed especially around 8 to 6 ka BP. The standard deviations of GDM_{LDC}, GDM_{EDML} and GDM_{GRIP} are 0.70 x10^{22}Am^2, 0.77 x10^{22}Am^2 and 1.06 x10^{22}Am^2, respectively. The standard deviations of GDM_{LDC} and GDM_{EDML} are significantly smaller than the standard deviation of the pfm9k2 model, i.e. 0.95 x10^{22}Am^2, despite that the radionuclide-based GDM are based on the same prior information with the pfm9k2 model. This result suggests a polar bias effect in the LDC and EDML ^{10}Be records that dampens the GDM influence by around 19% and 27%, respectively. These numbers are within the suggested range by Adolphi et al. (2023), i.e. 23% to 27%. On the contrary, the polar bias seems to be absent in the GRIP data suggesting

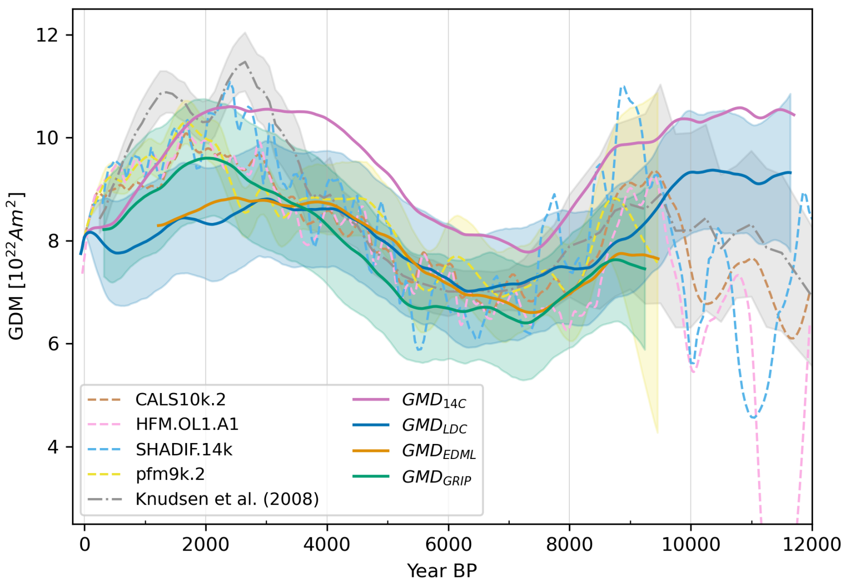

Figure 5.5: A comparison of Holocene GDM reconstructions from radionuclides (solid lines, see paper number 3) with independent GDM reconstructions from geomagnetic field models (dashed lines), i.e. CALS10k.2 and HFM.OL1.A1 (Constable et al., 2016), SHADIF.14k (Pavón-Carrasco et al., 2014), pfm9k.2 (Nilsson et al., 2022) and a Virtual Axial Dipole Moment (VADM, dashed-dotted line) reconstruction based on paleointensity data (Knudsen et al., 2008). The 2-σ uncertainties are indicated by the shadings with corresponding colours for GDM_{LDC}, GDM_{GRIP}, pfm9k.2 and the VADM.

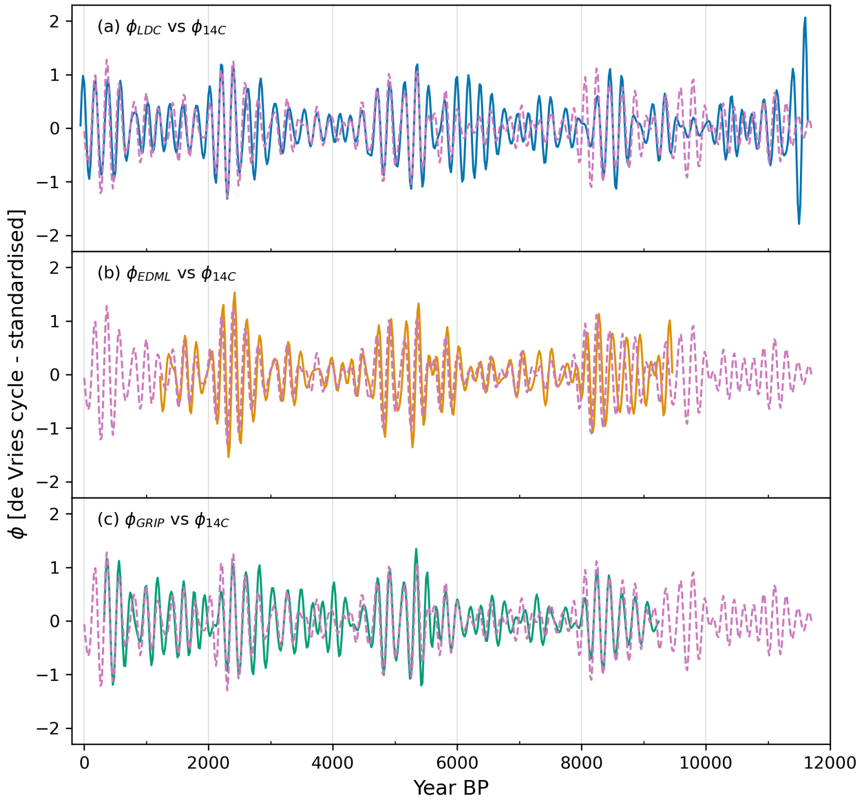

Figure 5.6: Comparisons of de Vries cycle amplitude based on ^{14}C to de Vries cycle based on the ^{10}Be concentrations of LDC (a), EDML (b) and GRIP (c). The standardised variations are at timescales between 180 to 250 years (see text).

that the site receives a rather well-mix global production ^{10}Be signal from both stratosphere and troposphere because any incomplete mixing scenarios will likely result in a polar bias (Adolphi et al., 2023). Overall, there is a clear difference in the mode of ^{10}Be transportation toward Greenland and Antarctica and also within Antarctica itself.

To evaluate the polar bias effects on solar reconstruction, I extracted de Vries (205- to 226-year) cycle (Damon & Sonett, 1991; Sonett & Suess, 1984) from the reconstructed solar activity based on LDC ^{10}Be concentration (ϕ_{LDC}), EDML ^{10}Be concentration (ϕ_{EDML}) and GRIP ^{10}Be concentration (ϕ_{GRIP}), and based on ^{14}C (ϕ_{14C}). A band-pass filter with cut-off frequencies of 1/180 year^{-1} and 1/250 year^{-1} was applied on the reconstructed ϕ to isolate de Vries cycle (figure 5.6). Before band-pass filtering, the data was standardised, i.e. the data mean was subtracted from the data which was then divided by its standard deviation. The cycle amplitude varies on millennial timescale as also suggested by previous studies (Dergachev & Vasiliev, 2019; McCracken et al., 2013; Steinhilber et al., 2012). The cycle amplitude in ϕ_{LDC} was clearly stronger than in ϕ_{14C} during the period from 7 to 6 ka BP. During this period ϕ_{14C}, ϕ_{GRIP} and ϕ_{EDML} exhibited a relatively weak de Vries cycle. The (standardised) standard deviation of de Vries cycle for the overlapping periods for all the reconstructions (9240 - 1220 years BP) are 0.48, 0.48, 0.44 and 0.43 for ϕ_{LDC}, ϕ_{EDML}, ϕ_{GRIP} and ϕ_{14C}, respectively. Assuming that the ^{14}C record reflects a well-mixed global production signal, ϕ_{LDC} and ϕ_{EDML} show enhanced variability by 5% (compared to ϕ_{14C}) while ϕ_{GRIP} shows only a small enhanced variability by 2%. This number of ϕ_{LDC} and ϕ_{EDML} are below the 7% - 8% polar bias enhancement suggested by Adolphi et al. (2023). The percentage of enhancement is relatively small considering the disagreements between ^{14}C and ^{10}Be (e.g. figure 5.6), and the potential effect of the carbon cycle on ϕ_{14C} (depending on the carbon cycle model one could possibly get different amplitudes in the ^{14}C production rate). Therefore, the effects of the polar bias on the reconstructed solar activity are uncertain and even if there are enhancement effects, the numbers are likely insignificant as shown by the results.

5.4 Prior information influences on long-term solar activity reconstruction

The Bayesian model utilises our knowledge on solar activity and GDM (in the form of prior distribution) and combines this knowledge with observations to deliver the intended result (in the form of posterior distribution). Uncertainty in the prior information can therefore affect the posterior distribution. Figure 5.7 shows the results of Holocene solar and geomagnetic field reconstructions from the Bayesian model based on two different prior information about the GDM variability (the priors for the solar activity were the same). ϕ_{LDC} and GDM_{LDC} (blue colours) are based on the same prior as the pfm9k.2 model while $\phi_{LDC.B}$ and $GDM_{LDC.B}$ (black colours) are based on the same prior as the pfm9k.2B model (Nilsson et al., 2022). The later prior allows for more GDM variations on timescales from 500 to 1000 years. This results in $GDM_{LDC.B}$ exhibiting more variations at this range than GDM_{LDC}. However, the pfm9k2.B prior is more conservative in terms of GDM variability on multi-millennial-scales as indicated by the 2-σ boundary of the prior in figure 5.7b. Consequently, the reconstructed $GDM_{LDC.B}$ is more constrained toward higher values than GDM_{LDC} during 8.5 to 5 ka BP. Lower values of $\phi_{LDC.B}$ were inferred by the Bayesian model to compensate for the higher GDM during this period. Figure 5.8 shows the results of a wavelet analysis (Torrence & Compo, 1998) of ϕ_{LDC} (a) and $\phi_{LDC.B}$ (b). ϕ_{LDC} has slightly more power in the periods from 500 to 1000 years compared to $\phi_{LDC.B}$ as indicated by the darker red regions in this variability range. These results illustrate a redistribution of the variations on timescales from 500 to 1000 years between the reconstructed GDM and ϕ by the Bayesian model depending on the prior information for the GDM variability. Although the prior knowledge is useful for disentangling solar activity and geomagnetic field influence on cosmogenic radionuclide, long-term solar reconstructions are still challenging due to the lack of knowledge of the Sun and GDM, especially their variations at the overlapping timescales. A potential solution is to verify the radionuclide-based GDMs to independent GDMs data in order to evaluate/adjust the prior information.

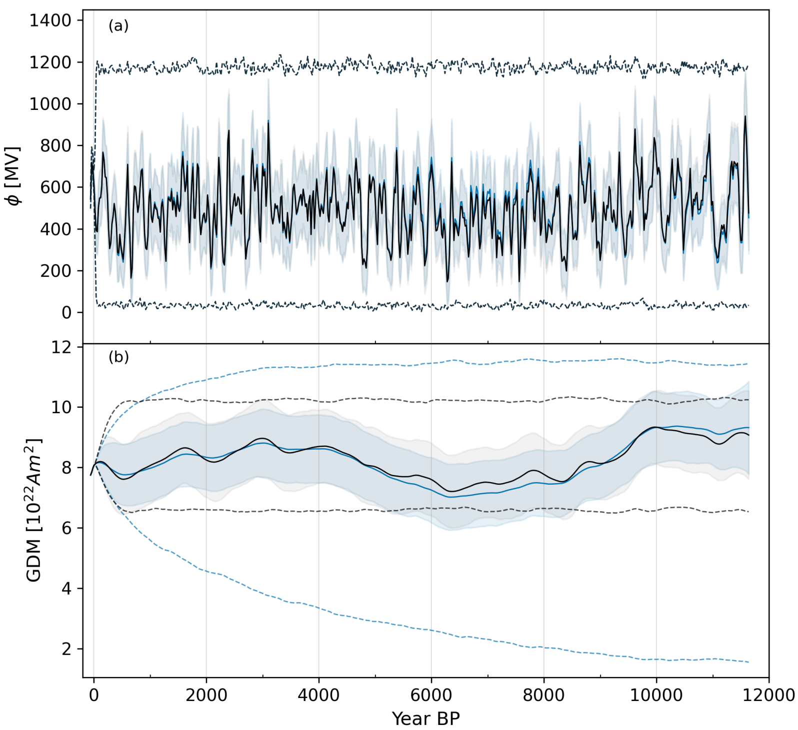

Figure 5.7: Holocene reconstructions of solar activity (a) and GDM (b) from the LDC ^{10}Be concentrations. The two reconstructions were conducted based on two different prior information on the GDM variability. The two priors are the same as the priors used for pfm9k.2 (blue colours) and pfm9k.2B (black colours) (Nilsson et al., 2022). The solid lines indicate the mean reconstruction. The dashed lines enclose the 2-σ uncertainty of the priors and the shadings indicate the 2-σ uncertainty of the reconstructions.

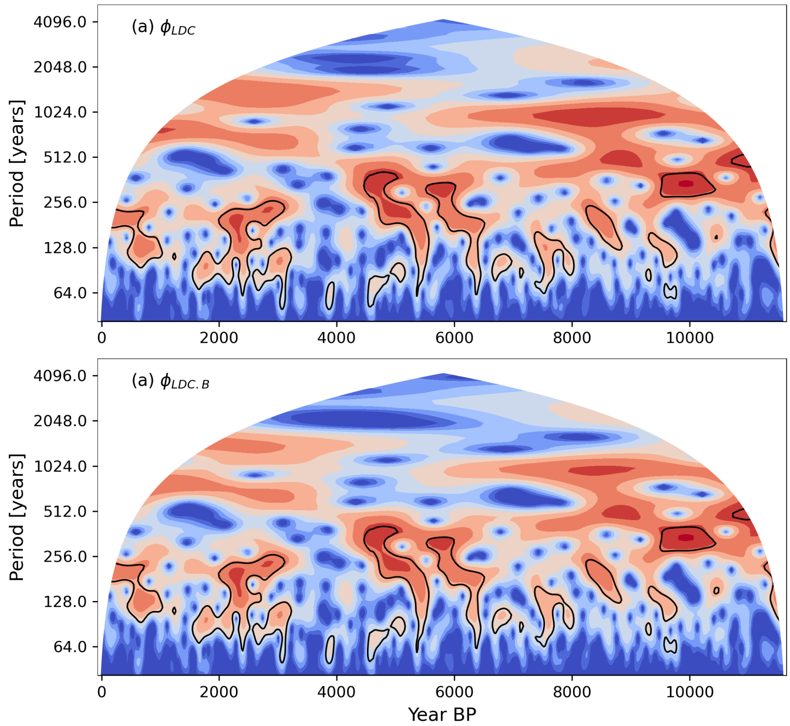

Figure 5.8: Wavelet analysis using the Morlet wavelet (Torrence & Compo, 1998) of two solar activity reconstructions ((a) ϕ_{LDC} and (b) $\phi_{LDC.B}$) using two different priors for the GDM (see text). The colour scales from low power (dark blue) to high power (dark red). The black contours enclose regions exceeding 95% confidence of the background noise which was estimated by a red-noise process with a lag-1 coefficient. The red-noise process is given as $X_t = \varphi * X_{t-1} + \varepsilon_t$ where φ is the lag-1 coefficient and ε_t is the white noise process with zero mean and constant variance σ_ε^2. The red-noise process is fitted to the data, i.e. ϕ_{LDC} and $\phi_{LDC.B}$.

6 Conclusions

The main focus of this PhD projects is to improve the reconstruction of Holocene solar activity (the last 11.7 ka). To do this, we have prepared and measured a new ^{10}Be record from Little Dome C (LDC), east Antarctica that covers the Holocene continuously. The record improves the quantity and quality of the currently global ^{10}Be dataset and therefore helps reduce data uncertainties of solar reconstructions. We also developed a new Bayesian model that can help to disentangle solar activity and geomagnetic field influences on cosmogenic radionuclide records. The model not only accounts for the variation characteristics but also eliminates the need for independent geomagnetic field reconstructions, that subsequently can be used to test the results. This further reduces the data noise and the uncertainty associated with the independent geomagnetic field reconstructions.

The new Bayesian model was applied to the new LDC ^{10}Be record and the existing long-term ^{10}Be records from the EDML and GRIP ice cores, and the ^{14}C production rate to reconstruct solar activity over the Holocene period. The decadal- and centennial-scale variations of solar activity can be consistently reconstructed from all the records. We found no firm evidences of multi-millennial-scale variations in solar activity which can be explained by the modelling approach. On the other hand, flaws in the modelling approach, such as systematic attribution of long-term solar activity to geomagnetic dipole moment (GDM) variability, would lead to consistent and systematic differences between the radionuclide-based GDM reconstructions and independent GDM reconstructions based on paleomagnetic data. However, we do not observe such consistent differences. Instead, we find long-term discrepancies among the different radionuclide-based and independent GDM reconstructions, especially for the last 4 ka. We also speculate that a polar bias effect could explain the dampened geomagnetic signal in the Antarctica ^{10}Be records (i.e. LDC and EDML) but also noted that there is no evidence for a polar bias in the GRIP ^{10}Be record. The long-term discrepancies among the ^{10}Be records results suggest a difference in the transport/deposition of ^{10}Be at ice core sites. In addition, the systematic difference between the ^{14}C data and all the ^{10}Be records is evidence for carbon cycle influences on the ^{14}C data. The reason is that the transportation/deposition processes are fundamentally different between ^{14}C (carbon cycle) and ^{10}Be (atmospheric circulation). Therefore, any systematic differences between them are most likely caused by the difference in the transportation/deposition processes.

Overall, the new LDC ^{10}Be data and the new Bayesian model resulted from this PhD project have brought new insights and a more complete picture of the solar activity during the Holocene epoch. The Sun varies persistently on centennial timescale (up to ~350-year periodicities) throughout the entire Holocene. However, the strength of the variations changes on millennial timescales. The variations were relatively weak around 2 to 1 ka BP, 4.5 to 3 ka BP and 8 to 6.4 ka BP and were strong otherwise. There is no evidence of long-term (multi-millennial-scale) increasing or decreasing trends in solar activity. These findings are important to understand the Sun-climate linkage and role of the Sun in millennial-scale climate changes. The results also improve our understanding on the present discrepancies among the ^{10}Be and the ^{14}C records and consequently the past changes in the carbon cycle.

Svensk sammanfattning

Rekonstruktioner av variationer i solens aktivitet under Holocen är viktiga för att förutsäga hur solen kommer att förändras i framtiden och för att förstå hur sådana variationer påverkar jordens klimat. För närvarande finns det skillnader mellan olika proxydata som används för att rekonstruera solaktivitet vars orsaker fortfarande är oklara. Detta leder till stora osäkerheter i holocena solaktivitetsrekonstruktioner. Det här doktorandprojektet syftar till att förbättra holocena solaktivitetsrekonstruktioner med nya mätningar och en bättre rekonstruktionsmetod. Resultaten är viktiga för sol- och solklimatstudier samt för en ökad förståelse av förändringar i kolets kretslopp under Holocen.

Kosmogena radionuklider som ^{10}Be i iskärnor och ^{14}C i trädringar är de vanligaste proxydata för att rekonstruera förändringar i solens aktivitet långt tillbaka i tiden. Koncentrationen av radionuklider i respektive arkiv återspeglar en kombination av produktions-, transport- och deponeringsprocesser (atmosfärisk cirkulation (^{10}Be) och kolcykeln (^{14}C)). För närvarande visar radionukliddata från olika iskärnor och trädringssekvenser skillnader i variationer på långa tidskalor (över tusentals år) som är svåra att förklara. Produktionen av radionuklider i atmosfären påverkas dessutom av variationer i jordens magnetfält som bara är delvis kända under Holocen. Detta leder till stora osäkerheter i rekonstruktioner av solaktiviteten på dessa tidskalor.

Den här avhandlingen är baserad på nya ^{10}Be-mätningar från 759 isprover från ett borrhål på Little Dome C (LDC), östra Antarktis. Den nya ^{10}Be-dataserien täcker kontinuerligt hela Holocen. En Bayesiansk modell utvecklades också för att separera förändringar i koncentrationen av ^{10}Be i isen som beror på variationer i solens aktivitet och jordens magnetfält. Modellen applicerades på de nya LDC ^{10}Be-mätningarna och även på befintliga ^{10}Be-data från andra iskärnor samt ^{14}C-data från trädringar. Rekonstruktionerna visar reproducerbara variationer i solaktivitet på tidskalor av tio till hundratalstals år medan variationer på tusentals år fortfarande är osäkra. Stora skillnader noteras framför allt mellan ^{10}Be-data och ^{14}C-data över de senaste 4000 åren. Vi hittade också indikationer på en så-kallad polär bias-effekt som kan förklara en dämpad inverkan av variationer i jordens magnetfält i ^{10}Be-data från Antarktis, men vi ser ingen antydning till en liknande effekt i data från det grönländska istäcket. De nya resultaten pekar på skillnader i transportprocesserna för ^{10}Be mot de olika depositionsplatserna i Arktis och Antarktis samt förändringar i kolcykeln under Holocen som påverkar ^{14}C-data.

References

Adolphi, F., Herbst, K., Nilsson, A., & Panovska, S. (2023). On the Polar Bias in Ice Core 10Be Data. *Journal of Geophysical Research: Atmospheres*, *128*(4), e2022JD038203. https://doi.org/10.1029/2022JD038203

Adolphi, F., & Muscheler, R. (2016). Synchronizing the Greenland ice core and radiocarbon timescales over the Holocene - Bayesian wiggle-matching of cosmogenic radionuclide records. *Climate of the Past*, *12*(1), 15–30. https://doi.org/10.5194/cp-12-15-2016

Adolphi, F., Muscheler, R., Svensson, A., Aldahan, A., Possnert, G., Beer, J., Sjolte, J., Björck, S., Matthes, K., & Thieblemont, R. (2014). Persistent link between solar activity and Greenland climate during the Last Glacial Maximum. *Nature Geoscience*, *7*(9), 662–666. https://doi.org/10.1038/NGEO2225

Aldahan, A. (1998). Sixty year 10Be record from Greenland and Antarctica. *P. Indian AS -Earth*, *107*, 139–147.

Alley, R. B. (1995). Changes in continental and sea-salt atmospheric loadings in central Greenland during the most recent deglaciation: model-based estimates. *Journal of Glaciology*, *41*(139), 503–514. https://doi.org/10.1017/S0022143000034845

Bard, E., Raisbeck, G. M., Yiou, F., Jouzel, J., & Francé, F. (1997). Solar modulation of cosmogenic nuclide production over the last millennium: comparison between 14 C and 10 Be records. In *Earth and Planetary Science Letters* (Vol. 150).

Beer, J., McCracken, K., & von Steiger, R. (2012). *Cosmogenic Radionuclides: Theory and Applications in the Terrestrial and Space Environments* (1st ed.). Springer Berlin Heidelberg. https://doi.org/10.1007/978-3-642-14651-0_5

Beer, J., Siegenthaler, U., Bonani, G., Finkel, R. C., Oeschger, H., Suter, M., & Wölfli, W. (1988). Information on past solar activity and geomagnetism from 10Be in the Camp Century ice core. *Nature*, *331*(6158), 675–679. https://doi.org/10.1038/331675a0

Bonanno, A., Schlattl, H., & Paternò, L. (2002). The age of the Sun and the relativistic corrections in the EOS. *Astronomy & Astrophysics*, *390*(3), 1115–1118. https://doi.org/10.1051/0004-6361:20020749

Bond, G., Kromer, B., Beer, J., Muscheler, R., Evans, M. N., Showers, W., Hoffmann, S., Lotti-Bond, R., Hajdas, I., & Bonani, G. (2001). Persistent solar influence on north atlantic climate during the Holocene. *Science*, *294*(5549), 2130–2136. https://doi.org/10.1126/science.106568

Caballero-Lopez, R. A., & Moraal, H. (2004). Limitations of the force field equation to describe cosmic ray modulation. *Journal of Geophysical Research: Space Physics*, *109*(A1), 1101. https://doi.org/10.1029/2003JA010098

Carpenter, B., Gelman, A., Hoffman, M. D., Lee, D., Goodrich, B., Betancourt, M., Brubaker, M. A., Guo, J., Li, P., & Riddell, A. (2017). Stan: A probabilistic programming language. *Journal of Statistical Software*, *76*(1), 1–32. https://doi.org/10.18637/jss.v076.i01

Christl, M., Maden, C., Kubik, P. W., Müller, A., Ivy-Ochs, S., Suter, M., & Synal, H. A. (2010). Carrier-free measurements of natural 10Be/9Be ratios at low energies. *Nuclear Instruments and Methods in Physics Research Section B: Beam Interactions with Materials and Atoms*, *268*(7–8), 726–729. https://doi.org/10.1016/J.NIMB.2009.10.015

Christl, M., Vockenhuber, C., Kubik, P. W., Wacker, L., Lachner, J., Alfimov, V., & Synal, H. A. (2013). The ETH Zurich AMS facilities: Performance parameters and reference materials. *Nuclear Instruments and Methods in Physics Research, Section B: Beam Interactions with Materials and Atoms*, *294*, 29–38. https://doi.org/10.1016/j.nimb.2012.03.004

Clette, F., & Lefèvre, L. (2016). The New Sunspot Number: Assembling All Corrections. *Solar Physics*, *291*(9–10), 2629–2651. https://doi.org/10.1007/s11207-016-1014-y

Constable, C., & Korte, M. (2015). Centennial- to Millennial-Scale Geomagnetic Field Variations. *Treatise on Geophysics: Second Edition*, *5*, 309–341. https://doi.org/10.1016/B978-0-444-53802-4.00103-2

Constable, C., Korte, M., & Panovska, S. (2016). Persistent high paleosecular variation activity in southern hemisphere for at least 10 000 years. *Earth and Planetary Science Letters*, *453*, 78–86. https://doi.org/10.1016/J.EPSL.2016.08.015

Cuffey, K. M., & Clow, G. D. (1997). Temperature, accumulation, and ice sheet elevation in central Greenland through the last deglacial transition.

Journal of Geophysical Research: Oceans, *102*(C12), 26383–26396. https://doi.org/10.1029/96JC03981

Cuffey, K. M., Clow, G. D., Alley, R. B., Stuiver, M., Waddington, E. D., & Saltus, R. W. (1995). Large Arctic Temperature Change at the Wisconsin-Holocene Glacial Transition. *Science*, *270*(5235), 455–458. https://doi.org/10.1126/SCIENCE.270.5235.455

Damon, P. E., & Sonett, C. P. (1991). Solar and Terrestrial Components of the Atmospheric 14C Variation Spectrum. In C. P. Sonett, M. S. Giampapa, & M. S. Matthews (Eds.), *The Sun in Time* (p. 360).

Dergachev, V. A., & Vasiliev, S. S. (2019). Long-term changes in the concentration of radiocarbon and the nature of the Hallstatt cycle. *Journal of Atmospheric and Solar-Terrestrial Physics*, *182*, 10–24. https://doi.org/10.1016/J.JASTP.2018.10.005

Field, C. v., Schmidt, G. A., Koch, D., & Salyk, C. (2006). Modeling production and climate-related impacts on 10Be concentration in ice cores. *Journal of Geophysical Research Atmospheres*, *111*(15). https://doi.org/10.1029/2005JD006410

Finkel, R. C., & Nishiizumi, K. (1997). Beryllium 10 concentrations in the Greenland Ice Sheet Project 2 ice core from 3-40 ka. *Journal of Geophysical Research: Oceans*, *102*(C12), 26699–26706. https://doi.org/10.1029/97JC01282

Fudge, T. J., Markle, B. R., Cuffey, K. M., Buizert, C., Taylor, K. C., Steig, E. J., Waddington, E. D., Conway, H., & Koutnik, M. (2016). Variable relationship between accumulation and temperature in West Antarctica for the past 31,000 years. *Geophysical Research Letters*, *43*(8), 3795–3803. https://doi.org/10.1002/2016GL068356

Gallet, Y., Genevey, A., le Goff, M., Warmé, N., Gran-Aymerich, J., & Lefèvre, A. (2009). On the use of archeology in geomagnetism, and vice-versa: Recent developments in archeomagnetism. *Comptes Rendus Physique*, *10*(7), 630–648. https://doi.org/10.1016/J.CRHY.2009.08.005

Gelman, A., Carlin, J. B., Stern, H. S., & Rubin, D. B. (2004). *Bayesian data analysis.* (2nd ed.). Chapman & Hall/CRC.

Gleeson, L. J., & Axford, W. I. (1968). Solar Modulation of Galactic Cosmic Rays. *ApJ*, *154*, 1011. https://doi.org/10.1086/149822

Gleissberg, W. (1965). The eighty-year cycle in auroral frequency numbers. *J. Brit. Astr. Assoc.*, *75*, 227.

Gleissberg, W., & Schove, D. J. (1958). *The eighty-year sunspot cycle*. British Astronomical Association.

Gray, L. J., Beer, J., Geller, M., Haigh, J. D., Lockwood, M., Matthes, K., Cubasch, U., Fleitmann, D., Harrison, G., Hood, L., Luterbacher, J., Meehl, G. A., Shindell, D., van Geel, B., & White, W. (2010). Solar influences on climate. *Reviews of Geophysics*, *48*(4). https://doi.org/10.1029/2009RG000282

Heikkilä, U., Beer, J., & Feichter, J. (2009). Meridional transport and deposition of atmospheric 10Be. *Atmospheric Chemistry and Physics*, *9*(2). https://doi.org/10.5194/acp-9-515-2009

Heikkilä, U., Shi, X., Phipps, S. J., & Smith, A. M. (2014). 10Be in late deglacial climate simulated by ECHAM5-HAM - Part 2: Isolating the solar signal from 10Be deposition. *Climate of the Past*, *10*(2), 687–696. https://doi.org/10.5194/CP-10-687-2014

Heikkilä, U., & Smith, A. M. (2013). Production rate and climate influences on the variability of 10Be deposition simulated by ECHAM5-HAM: Globally, in Greenland, and in Antarctica. *Journal of Geophysical Research Atmospheres*, *118*(6), 2506–2520. https://doi.org/10.1002/jgrd.50217

Hellio, G., & Gillet, N. (2018). Time-correlation-based regression of the geomagnetic field from archeological and sediment records. *Geophysical Journal International*, *214*(3), 1585–1607. https://doi.org/10.1093/GJI/GGY214

Herbst, K., Muscheler, R., & Heber, B. (2017). The new local interstellar spectra and their influence on the production rates of the cosmogenic radionuclides 10Be and 14C. *Journal of Geophysical Research: Space Physics*, *122*(1), 23–34. https://doi.org/10.1002/2016JA023207

Horiuchi, K., Ohta, A., Uchida, T., Matsuzaki, H., Shibata, Y., & Motoyama, H. (2007). Concentration of 10Be in an ice core from the Dome Fuji station, Eastern Antarctica: Preliminary results from 1500 to 1810 yr AD. *Nuclear Instruments and Methods in Physics Research, Section B: Beam Interactions with Materials and Atoms*. https://doi.org/10.1016/j.nimb.2007.01.306

Horiuchi, K., Uchida, T., Sakamoto, Y., Ohta, A., Matsuzaki, H., Shibata, Y., & Motoyama, H. (2008). Ice core record of 10Be over the past millennium from Dome Fuji, Antarctica: A new proxy record of past solar activity and a powerful tool for stratigraphic dating. *Quaternary Geochronology*, *3*(3), 253–261. https://doi.org/10.1016/j.quageo.2008.01.003

Hoyt, D. v., & Schatten, K. H. (1998). Group Sunspot Numbers: A New Solar Activity Reconstruction. *Solar Physics*, *181*(2), 491–491. https://doi.org/10.1023/A:1005056326158

Jordan, C. E., Dibb, J. E., & Finkel, R. C. (2003). 10Be/7Be tracer of atmospheric transport and stratosphere-troposphere exchange. *Journal of Geophysical Research: Atmospheres*, *108*(D8), 4234. https://doi.org/10.1029/2002JD002395

Knudsen, M. F., Riisager, P., Donadini, F., Snowball, I., Muscheler, R., Korhonen, K., & Pesonen, L. J. (2008). Variations in the geomagnetic dipole moment during the Holocene and the past 50 kyr. *Earth and Planetary Science Letters*, *272*(1–2), 319–329. https://doi.org/10.1016/J.EPSL.2008.04.048

Knudsen, M. F., Riisager, P., Jacobsen, B. H., Muscheler, R., Snowball, I., & Seidenkrantz, M. S. (2009). Taking the pulse of the Sun during the Holocene by joint analysis of 14C and 10Be. *Geophysical Research Letters*, *36*(16). https://doi.org/10.1029/2009GL039439

Korte, M., & Muscheler, R. (2012). Centennial to millennial geomagnetic field variations. *Journal of Space Weather and Space Climate*, *2*, A08. https://doi.org/10.1051/SWSC/2012006

Kovaltsov, G. A., Mishev, A., & Usoskin, I. G. (2012). A new model of cosmogenic production of radiocarbon 14 C in the atmosphere. *Earth and Planetary Science Letters*, *337–338*, 114–120. https://doi.org/10.1016/j.epsl.2012.05.036

Kovaltsov, G. A., & Usoskin, I. G. (2010). A new 3D numerical model of cosmogenic nuclide 10Be production in the atmosphere. *Earth and Planetary Science Letters*, *291*(1–4), 182–188. https://doi.org/10.1016/j.epsl.2010.01.011

Kutschera, W. (2013). Applications of accelerator mass spectrometry. *International Journal of Mass Spectrometry*, *349–350*(1), 203–218. https://doi.org/10.1016/j.ijms.2013.05.023

Lachner, J., Ploner, M., Steier, P., Sakaguchi, A., & Usui, A. (2020). Accumulation of ferromanganese crusts derived from carrier-free 10Be/9Be. *Nuclear Instruments and Methods in Physics Research Section B: Beam Interactions with Materials and Atoms*, *467*, 146–151. https://doi.org/10.1016/J.NIMB.2019.11.047

Laj, C., Kissel, C., Mazaud, A., Michel, E., Muscheler, R., & Beer, J. (2002). Geomagnetic field intensity, North Atlantic Deep Water circulation and atmospheric Δ14C during the last 50 kyr. *Earth and Planetary Science Letters*, *200*(1–2), 177–190. https://doi.org/10.1016/S0012-821X(02)00618-0

Lal, D., & Peters, B. (1967). *Cosmic Ray Produced Radioactivity on the Earth*. 551–612. https://doi.org/10.1007/978-3-642-46079-1_7

Lilien, D. A., Steinhage, D., Taylor, D., Parrenin, F., Ritz, C., Mulvaney, R., Martín, C., Yan, J. B., O'Neill, C., Frezzotti, M., Miller, H., Gogineni, P., Dahl-Jensen, D., & Eisen, O. (2021). Brief communication: New radar constraints support presence of ice older than 1.5 Myr at Little Dome C. *Cryosphere*, *15*(4), 1881–1888. https://doi.org/10.5194/TC-15-1881-2021

Masarik, J., & Beer, J. (1999). Simulation of particle fluxes and cosmogenic nuclide production in the Earth's atmosphere. *Journal of Geophysical Research*, *104*(10), 99–112.

Masarik, J., & Beer, J. (2009). An updated simulation of particle fluxes and cosmogenic nuclide production in the Earth's atmosphere. *Journal of Geophysical Research: Atmospheres*, *114*(D11), 11103. https://doi.org/10.1029/2008JD010557

McCracken, K. G. (2004). Geomagnetic and atmospheric effects upon the cosmogenic 10Be observed in polar ice. *Journal of Geophysical Research: Space Physics*, *109*(A4). https://doi.org/10.1029/2003JA010060

McHargue, L. R., & Damon, P. E. (1991). The global beryllium 10 cycle. *Reviews of Geophysics*, *29*(2), 141. https://doi.org/10.1029/91RG00072

Moraal, H. (2013). Cosmic-ray modulation equations. *Space Science Reviews*, *176*(1–4), 299–319. https://doi.org/10.1007/S11214-011-9819-3

Muscheler, R., Adolphi, F., Herbst, K., & Nilsson, A. (2016). The Revised Sunspot Record in Comparison to Cosmogenic Radionuclide-Based Solar Activity Reconstructions. *Solar Physics*, *291*(9–10), 3025–3043. https://doi.org/10.1007/s11207-016-0969-z

Muscheler, R., Beer, J., Kubik, P. W., & Synal, H. A. (2005). Geomagnetic field intensity during the last 60,000 years based on 10Be and 36Cl from the Summit ice cores and 14C. *Quaternary Science Reviews*, *24*(16–17), 1849–1860. https://doi.org/10.1016/j.quascirev.2005.01.012

Muscheler, R., Beer, J., Wagner, G., Laj, C., Kissel, C., Raisbeck, G. M., Yiou, F., & Kubik, P. W. (2004). Changes in the carbon cycle during the last deglaciation as indicated by the comparison of 10Be and 14C records. *Earth and Planetary Science Letters*, *219*(3–4), 325–340. https://doi.org/10.1016/S0012-821X(03)00722-2

Muscheler, R., & Heikkilä, U. (2011). Constraints on long-term changes in solar activity from the range of variability of cosmogenic radionuclide records. *Astrophysics and Space Sciences Transactions*, *7*(3), 355–364. https://doi.org/10.5194/ASTRA-7-355-2011

Muscheler, R., Joos, F., Beer, J., Müller, S. A., Vonmoos, M., & Snowball, I. (2007). Solar activity during the last 1000 yr inferred from radionuclide records. *Quaternary Science Reviews*, *26*(1–2), 82–97. https://doi.org/10.1016/j.quascirev.2006.07.012

NASA. (2017, August 4). *Solar Storm and Space Weather - Frequently Asked Questions*. https://www.nasa.gov/mission_pages/sunearth/spaceweather/index.html

Nguyen, L., Paleari, C. I., Müller, S., Christl, M., Mekhaldi, F., Gautschi, P., Mulvaney, R., Rix, J., & Muscheler, R. (2021). The potential for a continuous 10Be record measured on ice chips from a borehole. *Results in Geochemistry*, *5*(October), 100012. https://doi.org/10.1016/j.ringeo.2021.100012

Nguyen, L., Suttie, N., Nilsson, A., & Muscheler, R. (2022). A novel Bayesian approach for disentangling solar and geomagnetic field influences on the radionuclide production rates. *Earth, Planets and Space*, *74*(1), 1–19. https://doi.org/10.1186/S40623-022-01688-1

Nilsson, A., Holme, R., Korte, M., Suttie, N., & Hill, M. (2014). Reconstructing Holocene geomagnetic field variation: new methods, models and implications. *Geophysical Journal International Geophys. J. Int*, *198*, 229–248. https://doi.org/10.1093/gji/ggu120

Nilsson, A., & Suttie, N. (2021). Probabilistic approach to geomagnetic field modelling of data with age uncertainties and post-depositional magnetisations. *Physics of the Earth and Planetary Interiors*, *317*(February), 106737. https://doi.org/10.1016/j.pepi.2021.106737

Nilsson, A., Suttie, N., Stoner, J. S., & Muscheler, R. (2022). Recurrent ancient geomagnetic field anomalies shed light on future evolution of the South Atlantic Anomaly. *Proceedings of the National Academy of Sciences of the United States of America*, *119*(24), e2200749119. https://doi.org/10.1073/PNAS.2200749119

Owens, M. J., & Forsyth, R. J. (2013). The Heliospheric Magnetic Field. *Living Rev. Solar Phys*, *10*. https://doi.org/10.12942/lrsp-2013-5

Panovska, S., Korte, M., & Constable, C. G. (2019). One Hundred Thousand Years of Geomagnetic Field Evolution. In *Reviews of Geophysics* (Vol. 57, Issue 4, pp. 1289–1337). Blackwell Publishing Ltd. https://doi.org/10.1029/2019RG000656

Panovska, S., Korte, M., Finlay, C. C., & Constable, C. G. (2015). Limitations in paleomagnetic data and modelling techniques and their impact on Holocene geomagnetic field models. *Geophysical Journal International Geophys. J. Int*, *202*, 402–418. https://doi.org/10.1093/gji/ggv137

Parker, E. N. (1965). The passage of energetic charged particles through interplanetary space. *Planetary and Space Science*, *13*(1), 9–49. https://doi.org/10.1016/0032-0633(65)90131-5

Parrenin, F., Barnola, J., Beer, J., Blunier, T., Castellano, E., Chappellaz, J., Dreyfus, G., Fischer, H., Fujita, S., Jouzel, J., Kawamura, K., Lemieux-Dudon, B., Loulergue, L., Masson-Delmotte, V., Narcisi, B., Petit, J., Raisbeck, G., Raynaud, D., Ruth, U., … Wolff, E. (2007). The EDC3 chronology for the EPICA Dome C ice core. *Climate of the Past* , *3*, 485–497. www.clim-past.net/3/485/2007/

Pavón-Carrasco, F. J., Osete, M. L., Torta, J. M., & de Santis, A. (2014). A geomagnetic field model for the Holocene based on archaeomagnetic and lava flow data. *Earth and Planetary Science Letters*, *388*, 98–109. https://doi.org/10.1016/J.EPSL.2013.11.046

Pedro, J. B., Heikkilä, U. E., Klekociuk, A., Smith, A. M., van Ommen, T. D., & Curran, M. A. J. (2011). Beryllium-10 transport to Antarctica: Results from seasonally resolved observations and modeling. *Journal of Geophysical Research Atmospheres*, *116*(23). https://doi.org/10.1029/2011JD016530

Pedro, J. B., McConnell, J. R., van Ommen, T. D., Fink, D., Curran, M. A. J., Smith, A. M., Simon, K. J., Moy, A. D., & Das, S. B. (2012). Solar and climate influences on ice core 10Be records from Antarctica and Greenland during the neutron monitor era. *Earth and Planetary Science Letters*, *355–356*, 174–186. https://doi.org/10.1016/j.epsl.2012.08.038

Pedro, J. B., van Ommen, T., Curran, M., Morgan, V., Smith, A., & McMorrow, A. (2006). Evidence for climate modulation of the 10Be solar activity proxy. *Journal of Geophysical Research Atmospheres*, *111*(21). https://doi.org/10.1029/2005JD006764

Raisbeck, G. M., Cauquoin, A., Jouzel, J., Landais, A., Petit, J.-R., Lipenkov, V. Y., Beer, J., Synal, H.-A., Oerter, H., Johnsen, S. J., Steffensen, J. P., Svensson, A., & Yiou, F. (2017). An improved north–south synchronization of ice core records around the 41 kyr 10Be peak. *Climate of the Past*, *13*(3), 217–229. https://doi.org/10.5194/cp-13-217-2017

Raisbeck, G. M., Yiou, F., Bourles, D., Lorius, C., Jouzel, J., & Barkov, N. I. (1987). Evidence for two intervals of enhanced 10Be deposition in Antarctic ice during the last glacial period. *Nature*, *326*(6110), 273–277. https://doi.org/10.1038/326273a0

Raisbeck, G. M., Yiou, F., Cattani, O., & Jouzel, J. (2006). 10Be evidence for the Matuyama-Brunhes geomagnetic reversal in the EPICA Dome C ice core. *Nature*, *444*(7115), 82–84. https://doi.org/10.1038/nature05266

Raisbeck, G. M., Yiou, F., Fruneau, M., & Loiseaux, J. M. (1978). Beryllium-10 Mass Spectrometry with a Cyclotron. *Science*, *202*(4364), 215–217. http://www.jstor.org/stable/1746223

Raisbeck, G. M., Yiou, F., Fruneau, M., Loiseaux, J. M., Lieuvin, M., & Ravel, J. C. (1981a). Cosmogenic 10Be/7Be as a probe of atmospheric transport processes. *Geophysical Research Letters*, *8*(9), 1015–1018. https://doi.org/10.1029/GL008i009p01015

Raisbeck, G. M., Yiou, F., Fruneau, M., Loiseaux, J. M., Lieuvin, M., Ravel, J. C., & Lorius, C. (1981b). Cosmogenic 10Be concentrations in Antarctic ice during the past 30,000 years. *Nature*, *292*(5826), 825–826. https://doi.org/10.1038/292825a0

Raisbeck, G. M., Yiou, F., Jouzel, J., & Petit, J. R. (1990). 10 Be and δ 2 H in polar ice cores as a probe of the solar variability's influence on climate. *Philosophical Transactions of the Royal Society of London. Series A, Mathematical and Physical Sciences*, *330*(1615), 463–470. https://doi.org/10.1098/rsta.1990.0027

Raisbeck, G. M., Yiou, F., Jouzel, J., & Stocker, T. F. (2007). Direct north-south synchronization of abrupt climate change record in ice cores using Beryllium 10. *Climate of the Past*, *3*(3), 541–547. https://doi.org/10.5194/cp-3-541-2007

Reimer, P. J., Austin, W. E. N., Bard, E., Bayliss, A., Blackwell, P. G., Bronk Ramsey, C., Butzin, M., Cheng, H., Edwards, R. L., Friedrich, M., Grootes, P. M., Guilderson, T. P., Hajdas, I., Heaton, T. J., Hogg, A. G., Hughen, K. A., Kromer, B., Manning, S. W., Muscheler, R., … Talamo, S. (2020). The IntCal20 Northern Hemisphere Radiocarbon Age Calibration Curve (0–55 cal kBP). *Radiocarbon*, *62*(4), 725–757. https://doi.org/DOI: 10.1017/RDC.2020.41

Rix, J., Mulvaney, R., Hong, J., & Ashurst, D. A. N. (2019). Development of the British Antarctic Survey Rapid Access Isotope Drill. *Journal of Glaciology*, *65*(250), 288–298. https://doi.org/10.1017/jog.2019.9

Rowell, I. F., Mulvaney, R., Rix, J., Tetzner, D. R., & Wolff, E. W. (2022). Viability of chemical and water isotope ratio measurements of RAID ice chippings from Antarctica. *Journal of Glaciology 1–16*, 1–16. https://doi.org/10.1017/jog.2022.94

Schwabe, S. H. (1844). Sonnenbeobachtungen im Jahre 1843. *Dessau. Astron. Nachr.*, *21*, 223.

Siegenthaler, U. (1983). Uptake of excess CO2 by an outcrop-diffusion model of the ocean. *Journal of Geophysical Research*, *88*(C6), 3599–3608. https://doi.org/10.1029/JC088iC06p03599

Sigl, M., Fudge, T. J., Winstrup, M., Cole-Dai, J., Ferris, D., Mcconnell, J. R., Taylor, K. C., Welten, K. C., Woodruff, T. E., Adolphi, F., Bisiaux, M., Brook, E. J., Buizert, C., Caffee, M. W., Dunbar, N. W., Edwards, R., Geng, L., Iverson, N., Koffman, B., … Sowers, T. A. (2016). The WAIS Divide deep ice core WD2014 chronology-Part 2: Annual-layer counting (0-31 ka BP). *Climate of the Past*, *12*, 769–786. https://doi.org/10.5194/cp-12-769-2016

Simpson, J. A. (2000). The cosmic ray nucleonic component: The invention and scientific uses of the neutron monitor. *Space Science Reviews*, *93*(1–2), 11–32. https://doi.org/10.1023/A:1026567706183

Snowball, I., & Muscheler, R. (2007). Palaeomagnetic intensity data: an Achilles heel of solar activity reconstructions. *The Holocene*, *17*(6), 851–859. https://doi.org/10.1177/0959683607080531

Sonett, C. P., & Suess, H. E. (1984). Correlation of bristlecone pine ring widths with atmospheric 14C variations: a climate–Sun relation. *Nature 1984 307:5947*, *307*(5947), 141–143. https://doi.org/10.1038/307141a0

Steig, E. J., Polissar, P. J., Stuiver, M., Grootes, P. M., & Finkel, R. C. (1996). Large amplitude solar modulation cycles of 10Be in Antarctica: Implications for atmospheric mixing processes and interpretation of the ice core record. *Geophysical Research Letters*, *23*(5), 523–526. https://doi.org/10.1029/96GL00255

Steinhilber, F., Abreu, J. A., Beer, J., Brunner, I., Christl, M., Fischer, H., Heikkilä, U., Kubik, P. W., Mann, M., McCracken, K. G., Miller, H., Miyahara, H., Oerter, H., & Wilhelms, F. (2012). 9,400 Years of cosmic radiation and solar activity from ice cores and tree rings. *Proceedings of the National Academy of Sciences of the United States of America*, *109*(16), 5967–5971. https://doi.org/10.1073/pnas.1118965109

Stenni, B., Masson-Delmotte, V., Selmo, E., Oerter, H., Meyer, H., Röthlisberger, R., Jouzel, J., Cattani, O., Falourd, S., Fischer, H., Hoffmann, G., Iacumin, P., Johnsen, S. J., Minster, B., & Udisti, R. (2010). The deuterium excess records of EPICA Dome C and Dronning Maud Land ice cores (East Antarctica). *Quaternary Science Reviews*, *29*(1–2), 146–159. https://doi.org/10.1016/J.QUASCIREV.2009.10.009

Svalgaard, L., & Schatten, K. H. (2016). Reconstruction of the Sunspot Group Number: The Backbone Method. *Solar Physics*, *291*(9–10), 2653–2684. https://doi.org/10.1007/s11207-015-0815-8

Synal, H. A. (2013). Developments in accelerator mass spectrometry. *International Journal of Mass Spectrometry*, *349–350*(1), 192–202. https://doi.org/10.1016/j.ijms.2013.05.008

Torrence, C., & Compo, G. P. (1998). A Practical Guide to Wavelet Analysis. *Bulletin of the American Meteorological Society*, *79*(1), 61–78. https://doi.org/10.1175/1520-0477(1998)079

Usoskin, I. G., Gallet, Y., Lopes, F., Kovaltsov, G. A., & Hulot, G. (2016). Astrophysics Solar activity during the Holocene: the Hallstatt cycle and its consequence for grand minima and maxima. *A&A*, *587*, 150. https://doi.org/10.1051/0004-6361/201527295

Veres, D., Bazin, L., Landais, A., Toyé, H., Kele, M., Lemieux-Dudon, B., Parrenin, F., Martinerie, P., Blayo, E., Blunier, T., Capron, E., Chappellaz, J., Rasmussen, S. O., Severi, M., Svensson, A., & Wolff, E. W. (2013). The Antarctic ice core chronology (AICC2012): an optimized multi-parameter and multi-site dating approach for the last 120 thousand years. *Climate of the Past*, *9*, 1733–1748. https://doi.org/10.5194/cp-9-1733-2013

Vonmoos, M., Beer, J., & Muscheler, R. (2006). Large variations in Holocene solar activity: Constraints from 10Be in the Greenland Ice Core Project ice core. *Journal of Geophysical Research: Space Physics*, *111*(10), A10105. https://doi.org/10.1029/2005JA011500

Wagner, G., Beer, J., Masarik, J., Muscheler, R., Kubik, P. W., Mende, W., Laj, C., Raisbeck, G. M., & Yiou, F. (2001). Presence of the Solar de Vries Cycle (~205 years) during the Last Ice Age. *Geophysical Research Letters*, *28*(2), 303–306. https://doi.org/10.1029/2000GL006116

Wieler, R., Beer, J., & Leya, I. (2013). The Galactic Cosmic Ray Intensity over the Past 106–109 Years as Recorded by Cosmogenic Nuclides in Meteorites and Terrestrial Samples. *Space Science Reviews*, *176*(1–4), 351–363. https://doi.org/10.1007/s11214-011-9769-9

Wolf, R. (1851). Sonnenflecken Beobachtungen in der zweiten Hälfte des Jahres 1850. *Mitt. Nat. Forsch. Ges.*, *207*, 89–95.

Wolf, R. (1856). Beobachtungen der Sonnenflecken in den Jahren 1849–1855. *Astron. Mitteil. Eidgn. Sternw.*, *1*, 3–13.

Wu, C. J., Usoskin, I. G., Krivova, N., Kovaltsov, G. A., Baroni, M., Bard, E., & Solanki, S. K. (2018). Solar activity over nine millennia: A consistent multi-proxy reconstruction. *Astronomy and Astrophysics*, *615*(Usoskin 2017), 1–13. https://doi.org/10.1051/0004-6361/201731892

Yang, S., Odah, H., & Shaw, J. (2000). Variations in the geomagnetic dipole moment over the last 12000 years. *Geophysical Journal International*, *140*(1), 158–162. https://doi.org/10.1046/j.1365-246X.2000.00011.x

Yiou, F., Raisbeck, G. M., Baumgartner, S., Beer, J., Hammer, C., Johnsen, S., Jouzel, J., Kubik, P. W., Lestringuez, J., Stiévenard, M., Suter, M., & Yiou, P. (1997). Beryllium 10 in the Greenland Ice Core Project ice core at Summit, Greenland. *Journal of Geophysical Research: Oceans*, *102*(C12), 26783–26794. https://doi.org/10.1029/97JC01265

Zheng, M., Adolphi, F., Sjolte, J., Aldahan, A., Possnert, G., Wu, M., Chen, P., & Muscheler, R. (2021a). Solar Activity of the Past 100 Years Inferred From 10Be in Ice Cores—Implications for Long-Term Solar Activity Reconstructions. *Geophysical Research Letters*, *48*(4), e2020GL090896. https://doi.org/10.1029/2020GL090896

Zheng, M., Sturevik-Storm, A., Nilsson, A., Adolphi, F., Aldahan, A., Possnert, G., & Muscheler, R. (2021b). Geomagnetic dipole moment variations for the last glacial period inferred from cosmogenic radionuclides in Greenland ice cores via disentangling the climate and production signals. *Quaternary Science Reviews*, *258*, 106881. https://doi.org/10.1016/j.quascirev.2021.106881